PERFECTLY MATCHED LAYER (PML) FOR FINITE DIFFERENCE TIME DOMAIN (FDTD) COMPUTATIONS IN PIEZOELECTRIC CRYSTALS

PERFECTLY MATCHED LAYER (PML) FOR FINITE DIFFERENCE TIME DOMAIN (FDTD) COMPUTATIONS IN PIEZOELECTRIC CRYSTALS

By

Farid F. Chagla, B.Eng.

A Thesis
Submitted to the School of Graduate Studies
In Partial Fulfillment of the Requirements
for the Degree
Master of Applied Science

McMaster University

MASTER OF APPLIED SCIENCE (2005) MCMASTER UNIVERSITY
(Electrical Engineering) Hamilton, Ontario

TITLE: Perfectly Match Layer (PML) For Finite Difference Time Domain (FDTD) Computations In Piezoelectric Crystals

AUTHOR: Farid F. Chagla, B. Eng. (McMaster University)

SUPERVISOR: Dr. Peter M. Smith

NUMBER OF PAGES: VII, 89

Abstract

The Finite-Difference Time-Domain (FDTD) method has become a very powerful tool for the analysis of propagating electromagnetic waves. It involves the discretization of Maxwell's equations in both time and space that leads to a numerical solution of the wave propagation problem in the time domain. The technique's main benefits are that it permits the description of wave propagation in non-uniform media, it can easily accommodate a wide range of boundary conditions, and it can be used to model non-linear effects as well as the wave behaviour near localized structures or material defects.

In this study, we extend this technique to mechanical wave propagation in piezoelectric crystals. It is observed to give large reflection artefacts generated by the computational boundaries which interfere with the desired wave propagation. To solve this problem, the renowned absorbing boundary condition called perfectly matched layer (PML) is used. PML was first introduced in 1994 for electromagnetic wave propagation. Our research has further developed this idea for acoustic wave propagation in piezoelectric crystals.

The need to improve the large reflection artefacts by introducing a finite thickness PML has reduced acoustic wave reflection occurring due to practical errors to less than 0.5 %. However, it is found that PML can generate numerical instabilities in the calculation of acoustic fields in piezoelectric crystals. Theses observations are also discussed in this report.

Acknowledgements

I wish to express my deepest gratitude to Dr. Peter M. Smith, for his continuing support, guidance and supervision throughout this study. His excellent leadership and supervision provided a stimulating environment which resulted in outstanding researching atmosphere.

Finally, my special thanks goes to my parents, my brother, sister, brother-in-law and sister-in-law, for their support and encouragement.

Contents

List of Figures

Chapter 1

1. Introduction to Numerical Simulation Techniques

1.1. Introduction

Partial differential equations (PDE) are at the heart of understanding and modeling physics, engineering and other science problems. The wave phenomena observed in light, water and sound are modeled using PDEs. Traditionally, these phenomena would be experimented and observed to form the analytical theory. However, analytical solutions to these theories are rarely available except for some special cases.

Since these solutions are hard to obtain, numerical modeling must be performed in order to better understand the wave phenomena. Numerical modeling also reduces the time and cost of the design cycle. This is because the results can be obtained by running a simulation instead of tweaking parameters and repeating experiments over and over again. Also, there are cases when an experiment cannot be performed or is difficult to process. In these cases, numerical simulation provides a solution to this problem with a click of a button.

Numerical simulations are an insightful tool that visually present the wave traveling in the media of interest. Observing the propagation not only enhances

understanding of wave behavior but also allows one to introduce parameters that are possible in theory but cannot be experimentally observed.

With these aspirations in mind, much research has been performed on finding suitable techniques to numerically solve PDEs. Some history of this is presented in the following section.

1.2. History

Before 1960, the solution of partial differential equations (PDE) was obtained in closed form or by using mechanical calculators. More recently computers allowed frequency domain solutions to become available at remarkable speeds. There were two types of frequency domain methods used, one was the integral equations and the other was high-frequency asymptotic methods. Both of these methods were capable of solving highly sophisticated problems at that time [3].

Nevertheless, there were several difficulties observed with these methods. The integral equation method has the ability to solve complex structures but it must restrict the size of the electrical model that it can use, especially in cases when there were many details to include for the structural geometry to be simulated [3].

Over the last four decades much research has been performed to address these problems. Even after 40 years of effort, there are still some difficulties to incorporating

non-linear behavior that is required to simulate active devices. Hence, the scientific community began looking at other possibilities, such as time domain techniques.

Although, the time domain solutions for Maxwell's equation were first introduced in 1966 by Yee, they did not receive much attention until the 1980's. Since the 1990's, the methods have been continuously developed for all sorts of wave propagations, primarily due to their ability to handle non-linear behavior [3]. One of the most effective time domain techniques was introduced by Yee and is now known as the Finite Difference Time Domain (FDTD) method, and it is the primary focus of this thesis.

1.3. Scope of Thesis

The purpose of this thesis is to introduce the FDTD method as a numerical simulation technique for wave propagation in piezoelectric crystals. This technique was first developed for EM wave propagation and it has been extended to simulate acoustic wave propagation in elastic and anisotropic media. To give an insightful discussion of the FDTD technique, a brief review of the theory behind the wave propagation in electromagnetic, elastic and piezoelectric media is presented at the beginning of this thesis. Following this, a brief discussion of phase velocities is provided. Next, a theoretical overview of the FDTD method for the EM, elastic and piezoelectrics media is given. This is followed by the implementation of absorbing boundary conditions (ABC), more specifically the perfectly matched layer (PML), to EM, elastic and piezoelectric media. The following chapter discusses the stability problems that limit the use of FDTD

in piezoelectrics. Finally, a conclusion and a set of recommendations are provided to complete this Thesis.

Chapter 2

2. Wave Propagation

2.1. Introduction

One interacts with waves in everyday life. For example, speech is a wave propagation phenomenon. Telecommunication networks are another example. Various phenomena in physics, mathematics, and chemistry, among other areas, are best described by waves. Scientifically, a wave is described as a disturbance from an equilibrium condition that propagates from one point to another without the matter transporting itself. An example of this definition is the Mexican wave where people successively stand up and down in a stadium. In this example, the equilibrium condition is when the people are sitting down and the disturbance is when the people are standing up [11].

Generally, there are two types of waves, namely mechanical waves and non-mechanical waves. Mechanical waves, such as sound waves, require a medium to propagate while non-mechanical waves do not. One of the classical examples of non-mechanical waves are light waves. Details of mechanical and non-mechanical waves are discussed in the next section.

2.2. The Electromagnetic Field Equations

An electromagnetic (EM) wave propagates through space at the speed of light. It does not require a medium to travel through as it travels through empty space. EM waves can be generated via oscillatory electric charges, which radiate waves containing electric and magnetic fields that are orthogonal to each other as well as to the direction of wave propagation. Hence, EM waves are transverse waves in free space [12].

Maxwell introduced the fundamental EM field equations stated in equations (1) and (2). Also accompanying are linear constitutive equations that are given in equations (3) and (4).

$$-\nabla \times \mathbf{E} = \frac{\partial \mathbf{B}}{\partial t} \tag{1}$$

$$\nabla \times \mathbf{H} = \frac{\partial \mathbf{D}}{\partial t} + J_c + J_s \tag{2}$$

$$\mathbf{D} = \boldsymbol{\varepsilon} \cdot \mathbf{E} \tag{3}$$

$$\mathbf{B} = \boldsymbol{\mu} \cdot \mathbf{H} \tag{4}$$

where

E = Electric field intensity

H = Magnetic field intensity

D = Electric flux displacement density

B = Magnetic flux

J_c = Conduction current density

J_s = Source current density

ε = Permittivity

μ = Permeability

Equations (1) and (2) are expressed in the absence of a source and conduction currents in equations (5) and (6) by using equations (3) and (4).

$$-\nabla \times \mathbf{E} = \mu_o \frac{\partial \mathbf{H}}{\partial t} \tag{5}$$

$$\nabla \times \mathbf{H} = \varepsilon \frac{\partial \mathbf{E}}{\partial t} \tag{6}$$

2.3. Fundamentals of Acoustic Waves

Acoustics involve mechanical vibrations or deformations varying with time. At the microscopic (atomic) level there are various patterns of vibrational motion. Acoustic theory focuses on the medium's macroscopic properties that are at particle level often consisting of many atoms. Acoustic wave propagation can be described by using these macroscopic properties along with the mechanical vibrations [6].

2.3.1. Acoustic Wave Propagation

Wave propagation can be described by particle wave motion. Particles of an elastic medium can be thought of as nodes in a mass spring system. When there is any disturbance, the elastic material then results in wave propagation throughout the medium. An elastic wave comes from the interaction of distributed inertial and elastic forces, similar to the mass spring system.

The types of wave that may propagate are determined by both the material properties of the solid and its boundary conditions. Fig. 1 gives examples of various types of waves that may occur in a solid. In order to be able to analyze these waves, we employ components of particle motion, such as particle displacement, stress and strain [14].

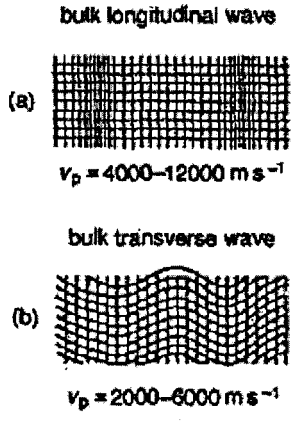

Figure 1: Elastic waves propagating in solids [14].

2.3.2. Displacement, Stress, and Strain

When force is applied to a solid it generates stress (T) within the solid. Stress in return then causes strain in a solid. Upon application of a force on the solid, the solid may deform, that is, alter its shape. Material deformation occurs when particles are displaced from their original position. Particle displacement can be described by using the displacement vector, which is a function of both time and space. An example of a displacement vector for an x-propagating plane wave is equation (7) [14].

$$\mathbf{u} = \mathbf{u}_o \exp(j(\omega t - \mathbf{k} \cdot \mathbf{x})) \qquad (7)$$

Where particle displacements $\mathbf{u}_o$ contains displacements in the three Cartesian coordinates. $\omega = 2\pi f$ is the angular frequency and $\mathbf{k}$ is the wave vector [14].

There are two kinds of plane waves in an isotropic medium. The first one has particle displacement that is parallel to the direction of propagation and is called the compressional wave. The second is the shear wave, which has particle displacement that is orthogonal to the direction of propagation. In the most general case there are two shear or transverse waves and one compressional wave. Fig. 2 pictorially depicts the two types of plane waves.

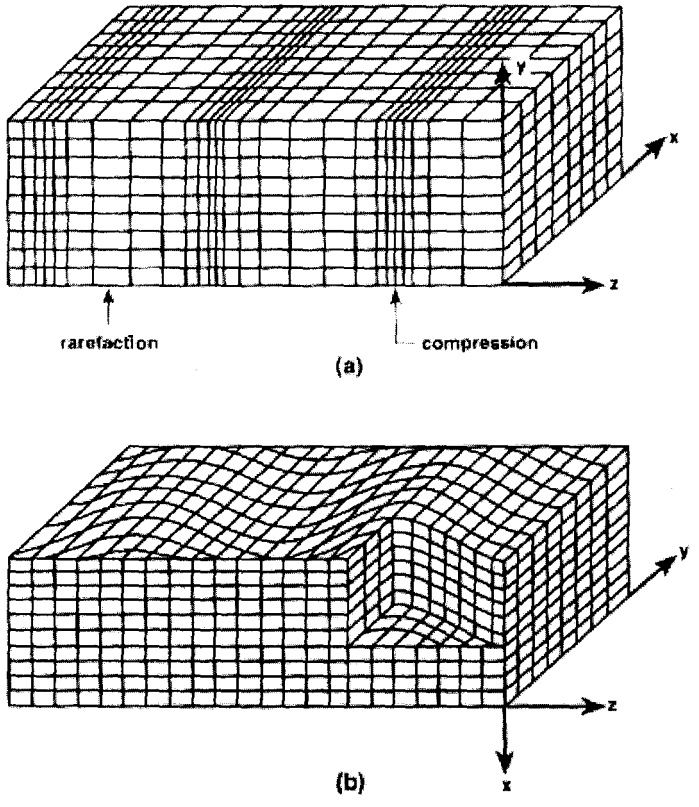

Figure 2: a) Compressional wave in solid b) Shear wave in a solid [14].

Wave propagation in a solid cannot involve rigid translation of the solid as a whole in which all particles move equally within the solid. An example of rigid translation is given in Fig. 3, which shows the whole body moved.

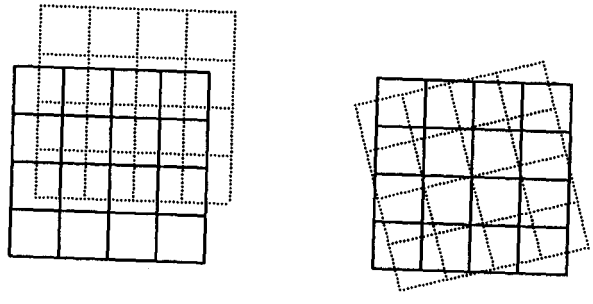

Figure 3: Rigid translation and rigid rotation.

For a wave to propagate through a medium, local deformation in a solid needs to exist. To observe and analyze local deformation and wave propagation, the displacement gradient is utilized. Equation (8) is a matrix formulation of the displacement gradient:

$$\nabla \mathbf{u} = \begin{pmatrix} \frac{\partial u_x}{\partial x} & \frac{\partial u_x}{\partial y} & \frac{\partial u_x}{\partial z} \\ \frac{\partial u_y}{\partial x} & \frac{\partial u_y}{\partial y} & \frac{\partial u_y}{\partial z} \\ \frac{\partial u_z}{\partial x} & \frac{\partial u_z}{\partial y} & \frac{\partial u_z}{\partial z} \end{pmatrix} \tag{8}$$

In equation (8), each element is written as $(\nabla u)_{ij} = \partial u_i / \partial x_j$ where i is the i^{th} displacement element and the derivative is taken with respect to j^{th} spatial coordinate [6]. Just like the translation of the entire body is not significant, similarly rigid rotation of the whole body is not of importance either, as it does not generate wave propagation. When equation 8 takes the gradient of the displacement vector it removes the effect of simple translation. Similarly, by summing the transpose of the displacement gradient to the displacement gradient itself, as given in equation (9), results in excluding any contribution of rigid rotation that may occur [6,14]:

$$S_{ij} = \frac{1}{2}\left(\frac{\partial u_i}{\partial x_j} + \frac{\partial u_j}{\partial x_i} \right) \tag{9}$$

where S_{ij} is called the strain.

Strain is defined as a change of length over unit length of the solid caused by an applied stress. The element S_{ii} represents axial strain in the i[th] direction and is known as compressional strain as well. The strain elements S_{ij} are known as shear strains when $i \neq j$ [14].

2.3.3. Equation of Motion and Elastic Constitutive Equations

Using Newton's 2[nd] law of motion F = ma as a basis, the equation of motion in solids can be developed. With the aid of Fig. 4, equation (11) describes the applied force in the x_1 or x axis [14].

$$F_1 = \{(T_{11} + \Delta T_{11})A_1 - T_{11}A_1\} + \{(T_{12} + \Delta T_{12})A_2 - T_{12}A_2\} + \{(T_{13} + \Delta T_{13})A_3 - T_{13}A_3\} \qquad (11)$$

where

F_1 is force(s) applied in the x direction

T_{11} is stress field located at normal to x plane while pointing in the x direction

ΔT_{11}, ΔT_{12}, ΔT_{13} is change in stress field by a small amount

A_1, A_2, A_3 is surface area of the sheet that is normal to x, y, z respectively

T_{12} is stress field component, normal to y plane while pointing in the x direction

T_{13} is stress field component, normal to z plane while pointing in the x direction

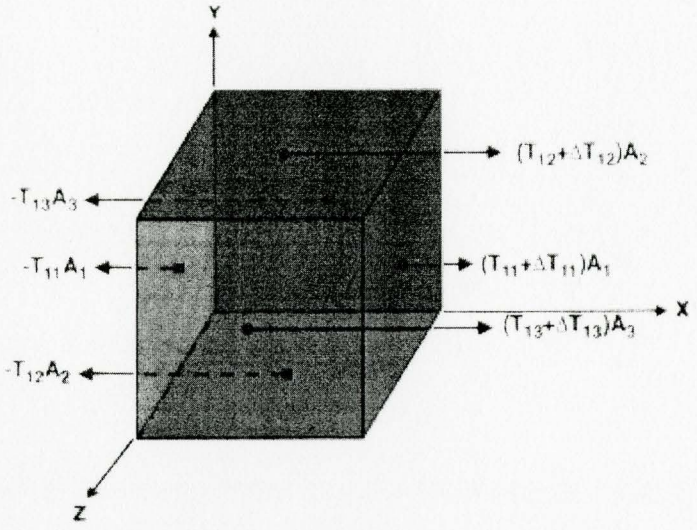

Figure 4: An elemental unit volume for an elastic solid [14].

For the force applied in equation (11), Newton's second law **F**=*m***a** can be used to develop an equation of motion. Substituting for mass with $m_v = \rho \triangle x \triangle y \triangle z$, where m_v is the elemental volume mass, ρ is the mass per volume (density), $\triangle x \triangle y \triangle z$ is an elemental volume and also substituting for acceleration $\mathbf{a} = \frac{\partial^2 \mathbf{u}}{\partial t^2}$ into Newton's second law we obtain equation (12).

$$\triangle T_{11} \triangle y \triangle z + \triangle T_{12} \triangle x \triangle z + \triangle T_{13} \triangle x \triangle y = \rho \triangle x \triangle y \triangle z \frac{\partial^2 u}{\partial t^2} \qquad (12)$$

Dividing equation (12) by $\triangle x \triangle y \triangle z$ and taking the infinitesimal limit gives the equation of motion:

$$\sum_{j=1}^{3} \frac{\partial T_{ij}}{\partial x_j} = \rho \frac{\partial^2 u_i}{\partial t^2} \tag{13}$$

A relationship between stress and strain can be established for the case of small deformations, for which stress is linearly proportional to the strain in a body. In one dimension, this can be thought of as Hooke's law, by relating the expansion and contraction of a spring or elastic material to the applied tensile force. In three dimensions, the relationship between stress and strain is given by the elastic constitutive relation, which is stated below:

$$T_{ij} = \sum_{k,l=1}^{3} c_{ijkl} S_{kl} \tag{14}$$

where c_{ijkl} are the elastic stiffness constants, which can be thought of as microscopic spring constants [6,14]. Since stress and strain are symmetric tensors, a more compact system in which two indices can be represented as one can be developed using abbreviated scripts.

2.3.4. Engineering Notation

Stress and other tensors are symmetric matrices and for this reason a compact system can be developed with new sets of notations that reduce two indices into one [14]. Table 1 shows the reduced index notation.

Index ij	Reduced Index I	Matrix Representation
11	1	$\begin{pmatrix} T_1 & T_6 & T_5 \\ T_6 & T_2 & T_4 \\ T_5 & T_4 & T_3 \end{pmatrix}$
22	2	
33	3	
23 or 32	4	
13 or 31	5	
12 or 21	6	

Table 1: Engineering notation or reduced notation index [14].

The elastic constitutive relations stated in equation (14) can be reduced with the engineering notation described in equation (15).

$$T_I = \sum_{J=1}^{6} c_{IJ} S_J \tag{15}$$

where I and J could vary from 1 to 6. The stiffness matrix c_{ijkl} could have $3^4 = 81$ elements, but again due to symmetries and use of reduced notation we get c_{ijkl} to become c_{IJ} which is used in equation (15). Since I and J vary from 1 to 6, this gives a total of 36 entries for the abbreviated stiffness matrix, instead of 81 elements.

Also, transforming strain equations (9) and (10) to abbreviated subscripts results in strain matrix expressed in equation (16).

$$\mathbf{S} = \nabla_s \mathbf{u} \tag{16}$$

where

$$\mathbf{S} = \begin{bmatrix} S_1 & S_2 & S_3 & S_4 & S_5 & S_6 \end{bmatrix}^T$$

$$\nabla_s = (\nabla \cdot)^T$$

$$\nabla \cdot = \begin{bmatrix} \frac{\partial}{\partial x} & 0 & 0 & 0 & \frac{\partial}{\partial z} & \frac{\partial}{\partial y} \\ 0 & \frac{\partial}{\partial y} & 0 & \frac{\partial}{\partial z} & 0 & \frac{\partial}{\partial x} \\ 0 & 0 & \frac{\partial}{\partial z} & \frac{\partial}{\partial y} & \frac{\partial}{\partial x} & 0 \end{bmatrix}$$

$$\mathbf{u} = \begin{bmatrix} u_x & u_y & u_z \end{bmatrix}^T$$

2.3.5. Wave Equation

By using the equation of motion (equation (13)) and also the elastic constitutive equation (equation (14)), the wave equation can be derived for plane waves propagating in elastic solids. Taking a spatial derivative of equation (14) results in equation (17):

$$\sum_{j=1}^{3} \frac{\partial T_{ij}}{\partial x_j} = \sum_{j,k,l=1}^{3} c_{ijkl} \frac{\partial S_{kl}}{\partial x_j} = \sum_{j,k,l=1}^{3} c_{ijkl} \frac{\partial^2 u_k}{\partial x_j \partial x_l} \tag{17}$$

where due to symmetry of strain matrix leads to $S_{kl} = \partial u_k / dx_1$ [14].

$$S_{ij} = \frac{1}{2}\left(\frac{\partial u_i}{\partial x_j} + \frac{\partial u_j}{\partial x_i} \right)$$

Combing the equation (17) with the equation of motion results in the wave equation (equation (18)):

$$\rho \frac{\partial^2 u_i}{\partial t^2} = \sum_{j,k,l=1}^{3} c_{ijkl} \frac{\partial^2 u_k}{\partial x_j \partial x_l} \tag{18}$$

where i =1, 2, 3 for the three particle displacements u [6].

An example of a wave propagating in the x direction is given in equation (19), which is one of the possible solutions of equation (18).

$$u_i(x,t) = u_o \exp(j\omega t - kx) \tag{19}$$

By placing this displacement solution into the wave equation for an isotropic media, it results in:

$$\begin{aligned} \rho \frac{\partial^2 u_1}{\partial t^2} &= c_{11} \frac{\partial^2 u_1}{\partial x^2} \Rightarrow \ \rho\omega^2 = c_{11}k^2 \\ \rho \frac{\partial^2 u_2}{\partial t^2} &= c_{44} \frac{\partial^2 u_2}{\partial x^2} \Rightarrow \rho\omega^2 = c_{44}k^2 \\ \rho \frac{\partial^2 u_3}{\partial t^2} &= c_{44} \frac{\partial^2 u_3}{\partial x^2} \Rightarrow \ \rho\omega^2 = c_{44}k^2 \end{aligned} \tag{20}$$

From equation (20), phase velocity ($v = \omega / k$) can be derived as

$$v_1 = \sqrt{c_{11}/\rho}$$

$$v_2 = v_3 = \sqrt{c_{44}/\rho} \tag{21}$$

where v_1 is the compressional wave velocity and $v_2 = v_3$ are the two shear wave velocities [14]. Further details of phase velocities are discussed in Chapter 3.

2.3.6. The Acoustic Field Equations

Another way to write equations (13) and (14) using abbreviated notation is given in equations (22) and (23),

$$\nabla \cdot \mathbf{T} = \rho \frac{\partial^2 \mathbf{u}}{\partial t^2} \tag{22}$$

$$\mathbf{T} = \mathbf{c} : \mathbf{S} \tag{23}$$

where : represents summation over abbreviated subscripts from equation (15).

Particle velocity stated in equation (24) is placed into equation (22) and (23) to obtain first order time derivatives.

$$\mathbf{v} = \frac{\partial \mathbf{u}}{\partial t} \tag{24}$$

$$\nabla \cdot \mathbf{T} = \rho \frac{\partial \mathbf{v}}{\partial t} \tag{25}$$

$$\nabla_s \mathbf{v} = \frac{\partial \mathbf{S}}{\partial t} \tag{26}$$

Taking the time derivative of equation (23) and placing equation (26) into the elastic constitutive equation gives

$$\mathbf{c} : \nabla_s \mathbf{v} = \frac{\partial \mathbf{T}}{\partial t} \tag{27}$$

Using equations (25) and (27), the wave propagation is expressed in terms of particle velocity and stress. Certain materials can get electrically polarized upon applied strain. These are called piezoelectric materials and require modification of equations (25) and (27) in order to describe the wave propagation in these media.

2.4. Piezoelectricity

Piezoelectricity provides the ability to drive mechanical waves using an electrical signal. Piezoelectricity occurs for certain materials that have electrical polarization and strain coupled to each other. When electrical polarization occurs for a crystal upon the application of strain, we refer to the behavior as direct piezoelectric effect. The converse effect is always present when there is the direct piezoelectric effect, and occurs when the application of an electric field results in strain. This is shown in Fig. 5 [14].

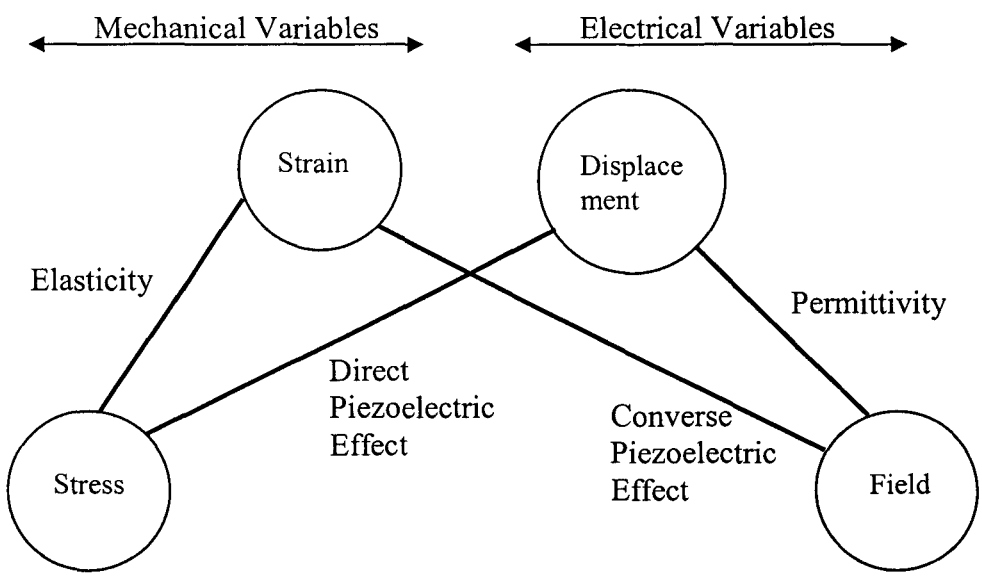

Figure 5: The coupling of electrical and mechanical variable for a crystal [14].

The piezoelectric effect is a linear phenomenon and is described in the following piezoelectric constitutive relations stated in equations (28) and (29):

$$T_I = c_{IJ}^E S_J - e_{Ij} E_j \tag{28}$$

$$D_i = \varepsilon_{ij}^S E_j + e_{iJ} S_J \tag{29}$$

where

e_{Ij}, e_{iJ} are piezoelectric stress constants

E is the electric field

D is the electrical displacement

c_{IJ}^E are the elastic stiffness constants (measured by keeping electric field constant)

ε_{ij}^S are the permittivity constants (measured with keeping strain constant)

The stress equation (28) for piezoelectric constitutive relations is a modified version of elastic constitutive relation in equation (23), where the piezoelectric constant times electric field is added [14].

Chapter 3

3. Phase Velocities and Slowness Curves

3.1. Introduction

The study of acoustic waves in piezoelectric materials depend on the media itself. All piezoelectric media are anisotropic materials. Anisotropic materials have various classes of crystals. The crystal classes are categorized by their elastic stiffness matrices, which are further discussed in the next section. The simplest method of studying acoustic wave behavior is by performing a plane wave analysis. The result of the analysis is the renowned Christoffel equation. With the aid of the Christoffel equation, phase velocities and inverse of phase velocities can be derived, which can provide insight into the acoustic plane wave behavior.

3.2. Crystal System

A crystal structure has atoms positioned in an ordered geometric pattern. For example, all atoms of a quartz crystal would have the same ordered geometric pattern. There are nine types of anisotropic crystal systems which are categorized by their microscopic properties. In Appendix 1, all nine classes of anisotropic crystal systems are listed. The microscopic properties of a media are given by the elastic stiffness constants c. The elastic constitutive equation contains these elastic stiffness constants, which can

be thought of as "the microscopic spring constants". Using abbreviated scripts reduces the elastic stiffness matrix c from a maximum of thirty six constants, to a maximum of twenty one [6]. When all twenty one constants are unique, it is classified as a Triclinic system. The minimum number of constants occurs for isotropic systems. An isotropic system requires only two independent constants for the c matrix, which fully describes elastic stiffness properties of the isotropic material. Using the appropriate elastic stiffness matrix, one can determine the possible solutions that may exist for plane waves in an acoustic media, as discussed in the following section.

3.3. Christoffel Equation

The lossless acoustic field equations are given in equations (25) and (27). For convenience they are repeated below.

$$\nabla \cdot \mathbf{T} = \rho \frac{\partial \mathbf{v}}{\partial t} \tag{30}$$

$$\mathbf{c} : \nabla_s \mathbf{v} = \frac{\partial \mathbf{T}}{\partial t} \tag{31}$$

where single dot product of del operator with stress is performed in equation (30) while equation (31) has double dot product. The symbol ∇ is the del operator defined in equation (34) and ∇_s is the transpose of this del operator [6].

The wave equation in terms of particle velocity v can be derived as,

$$\nabla \cdot \mathbf{c} : \nabla_s \mathbf{v} = \rho \frac{\partial^2 \mathbf{v}}{\partial t^2} \tag{32}$$

and in matrix form with abbreviated subscripts as [6],

$$\nabla_{iK} c_{KL} \nabla_{Lj} v_j = \rho \frac{\partial^2 v_i}{\partial t^2} \tag{33}$$

where v_j are the particle velocities, and the operators ∇_{iK}, and ∇_{Lj} are defined as [6]

$$\nabla_{iK} = \left(\nabla_{Lj}\right)^T = \begin{bmatrix} \frac{\partial}{\partial x} & 0 & 0 & 0 & \frac{\partial}{\partial z} & \frac{\partial}{\partial y} \\ 0 & \frac{\partial}{\partial y} & 0 & \frac{\partial}{\partial z} & 0 & \frac{\partial}{\partial x} \\ 0 & 0 & \frac{\partial}{\partial z} & \frac{\partial}{\partial y} & \frac{\partial}{\partial x} & 0 \end{bmatrix} \tag{34}$$

For an arbitrary uniform plane wave propagating in the [6]

$$\hat{l} = l_x \hat{x} + l_y \hat{y} + l_z \hat{z} \tag{35}$$

direction, the fields of the plane wave will be proportional to $\exp\left(j\left(\omega t - \mathbf{k}\hat{l} \cdot \mathbf{r}\right)\right)$. The operator ∇_{iK} in equation (34) can be replaced by,

$$-jk_{iK} = -jkl_{iK} = -jk\begin{bmatrix} l_x & 0 & 0 & 0 & l_z & l_y \\ 0 & l_y & 0 & l_z & 0 & l_x \\ 0 & 0 & l_z & l_y & l_x & 0 \end{bmatrix} \tag{36}$$

and similarly the operator ∇_{Lj} can be replaced by, [6]

$$-jk_{Lj} = -jkl_{Lj} = -jk\left(l_{iK}\right)^T \tag{37}$$

With these substitutions, the wave equation (31) reduces to [6]

$$k^2\left(l_{iK}c_{KL}l_{Lj}\right)v_j = k^2\Gamma_{ij}v_j = \rho\omega^2 v_i \tag{38}$$

Equation (38) is the well known Christoffel equation and the matrix Γ_{ij} is known as the Christoffel matrix. The elements of the Christoffel matrix are a function of the propagation direction and the medium's stiffness constants.

In Chapter 2, the wave equation for isotropic media provided the phase velocities, which are repeated below for convenience.

$$v_1 = \sqrt{c_{11}/\rho}$$

$$v_2 = v_3 = \sqrt{c_{44}/\rho} \tag{39}$$

where v_1 is the compressional wave velocity and $v_2 = v_3$ are the shear wave velocities [2]. The same result can be achieved by solving the Christoffel equation. The

parameters for an isotropic material are stated in equations (40) and (41), where equation (40) provides the elastic stiffness matrix c, and equation (41) describes the isotropy condition. Substituting these two expressions into the general Christoffel equation (38) gives the Christoffel equation for isotropic material, as stated in equation (42) [6].

$$\begin{bmatrix} c_{11} & c_{12} & c_{12} & 0 & 0 & 0 \\ c_{12} & c_{11} & c_{12} & 0 & 0 & 0 \\ c_{12} & c_{12} & c_{11} & 0 & 0 & 0 \\ 0 & 0 & 0 & c_{44} & 0 & 0 \\ 0 & 0 & 0 & 0 & c_{44} & 0 \\ 0 & 0 & 0 & 0 & 0 & c_{44} \end{bmatrix} \tag{40}$$

$$c_{12} = c_{11} - 2c_{44} \tag{41}$$

$$\left[\Gamma_{ij}\right] = \begin{bmatrix} c_{11}l_x^2 + c_{44}(1-l_x^2) & (c_{12}+c_{44})l_x l_y & (c_{12}+c_{44})l_x l_z \\ (c_{12}+c_{44})l_x l_y & c_{11}l_y^2 + c_{44}(1-l_y^2) & (c_{12}+c_{44})l_y l_z \\ (c_{12}+c_{44})l_x l_z & (c_{12}+c_{44})l_y l_z & c_{11}l_z^2 + c_{44}(1-l_z^2) \end{bmatrix} \tag{42}$$

Choosing the wave propagating direction as the x direction results in [6]:

$$k^2 \begin{bmatrix} c_{11} & 0 & 0 \\ 0 & c_{44} & 0 \\ 0 & 0 & c_{44} \end{bmatrix} \begin{bmatrix} v_x \\ v_y \\ v_z \end{bmatrix} = \rho\omega^2 \begin{bmatrix} v_x \\ v_y \\ v_z \end{bmatrix} \tag{43}$$

Expanding the equation gives three independent equations (44), (45), and (46) [6].

$$k^2 c_{11} v_x = \rho\omega^2 v_x \tag{44}$$

$$k^2 c_{44} v_y = \rho \omega^2 v_y \tag{45}$$

$$k^2 c_{44} v_z = \rho \omega^2 v_z \tag{46}$$

Since the direction of propagation is x, equation (44) gives the compressional wave velocity in equation (47). Equations (45) and (46) result in the two shear phase velocities as stated in equation (48) [6].

$$v_1 = k / \omega = \sqrt{\rho / c_{11}} \tag{47}$$

$$v_1 = v_2 = k / \omega = \sqrt{\rho / c_{44}} \tag{48}$$

These phase velocities are identical to those obtained in the example of Chapter 2, which was obtained by directly solving the wave equation.

To calculate the characteristics of any anisotropic solid, equation (38) is modified to give the general Christoffel equation for anisotropic media [6]:

$$\left[k^2 \Gamma_{i,j} - \rho \omega^2 \delta_{ij} \right] \left[v_j \right] = 0 \tag{49}$$

The characteristic determinant of equation (49) must be set to zero for non-trivial solutions. This gives the dispersion relation [6]

$$\Omega\left(w, k_x, k_y, k_z \right) = \left| k^2 \Gamma_{i,j} \left(l_x, l_y, l_z \right) - \rho \omega^2 \delta_{ij} \right| = 0 \tag{50}$$

At a given radian frequency ω, equation (50) defines a k-space surface Ω known as the wave vector surface, which gives k as a function of direction $\hat{l}$. This dispersion relation can also be expressed as a variable k/ω, which is known as the inverse phase velocity or as the slowness. The slowness curve does not depend on ω, and therefore is the preferred parameter. Further details of slowness curves are discussed in the following section.

In Chapter F of [6], derivations of Christoffel equations are performed. The result of the analysis is that the Christoffel equation for piezoelectric media has exactly the same form as that of anisotropic media stated in equation (49), except that piezoelectric stiffened elastic constants given in equation (51) take the place of anisotropic stiffness constants

$$c_{KL} \rightarrow \left\{ c_{KL}^{E} + \frac{\left[e_{Kj} l_j\right]\left[l_i e_{iL}\right]}{l_i \varepsilon_{ij}^{S} l_j} \right\} \tag{51}$$

The overall solutions in piezoelectric solids correspond to the three uniform plane waves, namely the compressional and the two shear waves.

3.4. Slowness Curves

The three solutions of uniform plane waves can be plotted as a function of their direction, giving us the slowness curves. An example of a slowness curve for Bismuth

Germanium Oxide is shown in Fig. 6. The innermost curve corresponds to the quasi-longitudinal wave. The outermost curve corresponds to the quasi-slow-shear wave, while the middle curve corresponds to the quasi-fast-shear wave. For isotropic media, there are always pure modes of waves, only the anisotropic media have quasi modes. A pure mode occurs when the wave solutions are either parallel or transverse to the direction of propagation. The quasi modes have wave solutions that are not exactly parallel or exactly transverse to the direction of propagation.

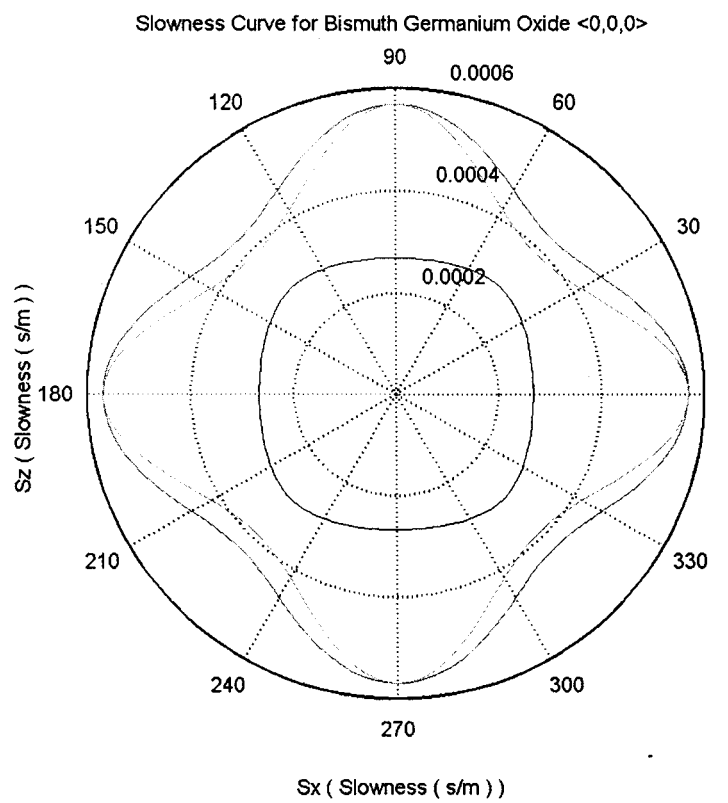

Figure 6: Slowness Curve for x-z plane in Bismuth Germanium Oxide.

Chapter 4

4. Finite Difference Time Domain (FDTD)

4.1. Introduction

The Finite Difference Time Domain (FDTD) algorithm is a standard method for numerically solving a partial differential equation. Yee first applied it to electromagnetic wave propagation in 1966, after which it was extended to other fields, such as elastic and piezoelectric media. One benefit of this technique is that it permits the description of wave propagation in non-uniform media and can accommodate arbitrary boundary conditions. It also allows the study of non-linear behavior and the effects of localized structures or defects on wave propagation. This chapter presents a detailed discussion on applying FDTD in EM, elastic, and piezoelectric media.

4.2. FDTD applied to EM

Over the last few decades, the finite-difference time-domain (FDTD) method has been intensely researched to simulate EM wave propagation. This technique involves discretizing Maxwell's equations in time and space, resulting in a numerical solution for wave propagation.

Maxwell's equations for isotropic and dispersion free media are

$$-\nabla \times \mathbf{E} = \mu_o \frac{\partial \mathbf{H}}{\partial t} + \sigma_m \mathbf{H} + J_m \tag{52}$$

$$\nabla \times \mathbf{H} = \varepsilon \frac{\partial \mathbf{E}}{\partial t} + \sigma_e \mathbf{E} + J_e \tag{53}$$

In rectangular coordinate, these equations become

$$\mu \frac{\partial H_x}{\partial t} + \sigma_m H_x = -\left(\frac{\partial E_z}{\partial y} - \frac{\partial E_y}{\partial z} \right) - J_{mx} \tag{54}$$

$$\mu \frac{\partial H_y}{\partial t} + \sigma_m H_y = -\left(\frac{\partial E_x}{\partial z} - \frac{\partial E_z}{\partial x} \right) - J_{my} \tag{55}$$

$$\mu \frac{\partial H_z}{\partial t} + \sigma_m H_z = -\left(\frac{\partial E_y}{\partial x} - \frac{\partial E_x}{\partial y} \right) - J_{mz} \tag{56}$$

$$\varepsilon \frac{\partial E_x}{\partial t} + \sigma_e E_x = \frac{\partial H_z}{\partial y} - \frac{\partial H_y}{\partial z} - J_{ex} \tag{57}$$

$$\varepsilon \frac{\partial E_y}{\partial t} + \sigma_e E_y = \frac{\partial H_x}{\partial z} - \frac{\partial H_z}{\partial x} - J_{ey} \tag{58}$$

$$\varepsilon \frac{\partial E_z}{\partial t} + \sigma_e E_z = \frac{\partial H_y}{\partial x} - \frac{\partial H_x}{\partial y} - J_{ez} \tag{59}$$

Upon examining these differential equations, it is observed that the time derivative of E is dependent on the curl of H, and that the time derivative of H is dependent on the curl

of E. This interdependency is used to iterate through time and space, evaluating and updating field values.

For time discretization, the leap frog method is used. This method, depicted in Fig. 7, discretizes one of the fields at half-time instance. While iterating through time, it needs to store in memory all the E values computed at half-time instances. The H values at the next integer time instance will need them for updating all its field values. Similarly, once all the H values are calculated, they will also be stored in memory, since at the next half-time instance these values will be used to compute the new E field values. This way, E and H values are computed interdependently over time.

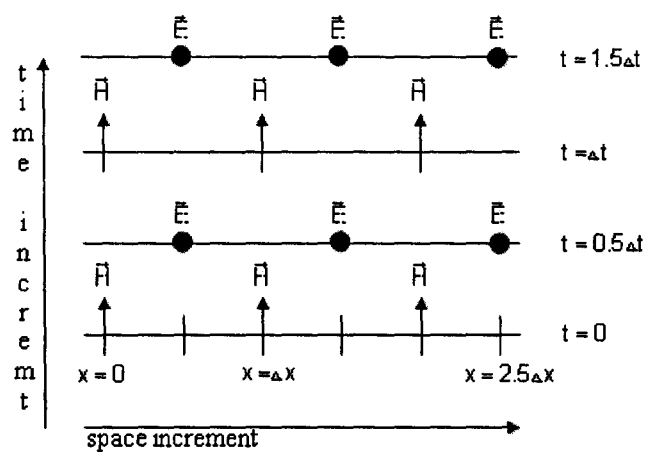

Figure 7: E and H discretization using leap frog method in 1-D.

To spatially discretize the computational domain, Kane Yee introduced an innovative method in 1966. He creatively used Maxwell's differential equations to divide the spatial domain into a cell, which he named Yee's cell. This cell places E components in such a manner that it can be surrounded by four circulating H components. And in a similar

manner, all its H field components are placed so that each is surrounded by four circulating E components, constructing a cell that implements the curl operation for E and H [3].

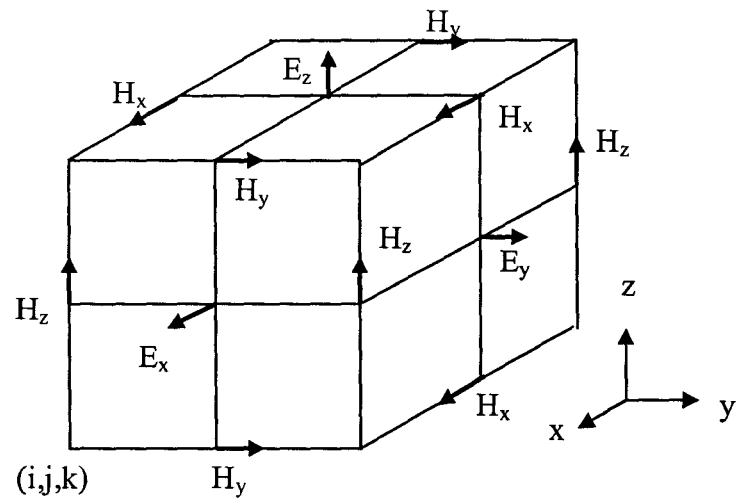

Figure 8: Yee's Cell, which visualizes the discretization of Maxwell's differential equations [5].

A 2-D TEz (TE mode propagating in z direction) for an isotropic and magnetic source free region is used to illustrate the FDTD technique. A Yee's cell for this mode is shown in Fig. 9. It is noteworthy that the field components are located at a distance of half a spatial increment away from one another.

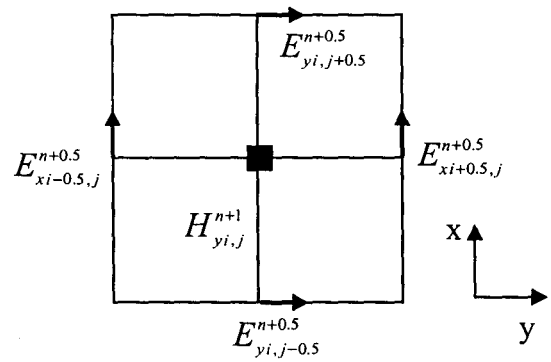

Figure 9: Yee's cell for 2-D TE_z.

With this visual aid, field equations are discretized using central differencing. The resulting equations are given below.

$$H^{n+1}_{zi,j} = \left[\frac{1-\frac{\sigma_m \Delta t}{2\mu}}{1+\frac{\sigma_m \Delta t}{2\mu}}\right] H^{n}_{zi,j} - \left[\frac{\frac{\Delta t}{\mu}}{1+\frac{\sigma_m \Delta t}{2\mu}}\right]\left[\frac{E^{n+0.5}_{yi+0.5,j} - E^{n+0.5}_{yi-0.5,j}}{\Delta x} - \frac{E^{n+0.5}_{xi,j+0.5} - E^{n+0.5}_{xi,j-0.5}}{\Delta y}\right] \quad (60)$$

$$E^{n+0.5}_{xi,j+0.5} = \left[\frac{1-\frac{\sigma_e \Delta t}{2\varepsilon}}{1+\frac{\sigma_e \Delta t}{2\varepsilon}}\right] E^{n-0.5}_{xi,j+0.5} + \left[\frac{\frac{\Delta t}{\varepsilon}}{1+\frac{\sigma_e \Delta t}{2\varepsilon}}\right]\left[\frac{H^{n}_{zi,j} - H^{n}_{zi,j-1}}{\Delta y} - J^{n+0.5}_{ex\,i,j+0.5}\right] \quad (61)$$

$$E^{n+0.5}_{yi+0.5,j} = \left[\frac{1-\frac{\sigma_e \Delta t}{2\varepsilon}}{1+\frac{\sigma_e \Delta t}{2\varepsilon}}\right] E^{n-0.5}_{yi+0.5,j} + \left[\frac{\frac{\Delta t}{\varepsilon}}{1+\frac{\sigma_e \Delta t}{2\varepsilon}}\right]\left[-\frac{H^{n}_{zi,j} - H^{n}_{zi-1,j}}{\Delta x} - J^{n+0.5}_{ey\,i+0.5,j}\right] \quad (62)$$

These FDTD equations face a stability criterion that is known as Courant stability. The time step interval must be less than or equal to the ratio of the grid cell size over the largest phase velocity. The grid cell size is usually taken to be one-twentieth of the

wavelength. This stability criterion, which is dependent on the number of dimensions of simulating space, is stated below:

$$1-\mathrm{D} \Rightarrow \Delta t \leq \frac{1}{V_p \sqrt{\frac{1}{(\Delta x)^2}}} \tag{63}$$

$$2-\mathrm{D} \Rightarrow \Delta t \leq \frac{1}{V_p \sqrt{\frac{1}{(\Delta x)^2}+\frac{1}{(\Delta y)^2}}} \tag{64}$$

$$3-\mathrm{D} \Rightarrow \Delta t \leq \frac{1}{V_p \sqrt{\frac{1}{(\Delta x)^2}+\frac{1}{(\Delta y)^2}+\frac{1}{(\Delta z)^2}}} \tag{65}$$

A demonstration for the successful implementation of the FDTD method is displayed in Fig. 10 with a few snapshots of the E and H fields. The wave is excited by a point source with a sinusoidal signal.

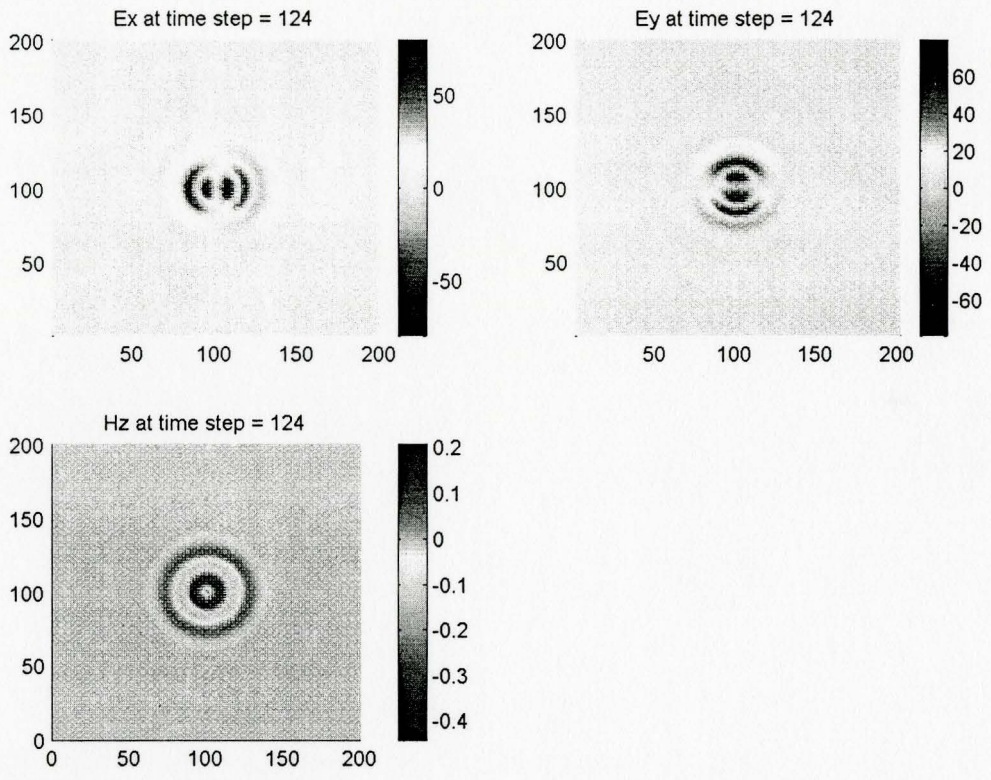

Figure 10: Snapshots of TE_z mode.

The successful implementation of the FDTD in electromagnetics has swiftly led to extending this technique to simulating other media. The following section includes a detailed discussion of the FDTD in elastic media.

4.3. FDTD Applied to Elastic Media

Similar to EM, the FDTD algorithm can be applied to simulate acoustic wave propagation in elastic media. In 1976, Madariaga was the first person to use the FDTD technique effectively to simulate acoustic waves in elastic media [10]. Her work applied the FDTD technique to acoustic wave equations that were expressed in terms of velocity

and stress. These equations, developed in Chapter 2, are repeated below for convenience. Madariaga's simulation used isotropic elastic material to simulate the acoustic waves with the FDTD method. The parameters required to describe an isotropic media are the isotropic elastic equations, the stiffness matrix given in equation (68), and the condition of isotropy expressed in equation (69).

$$\nabla \cdot \mathbf{T} = \rho \frac{\partial \mathbf{v}}{\partial t} \tag{66}$$

$$\mathbf{c} : \nabla_s \mathbf{v} = \frac{\partial \mathbf{T}}{\partial t} \tag{67}$$

$$\begin{bmatrix} c_{11} & c_{12} & c_{12} & 0 & 0 & 0 \\ c_{12} & c_{11} & c_{12} & 0 & 0 & 0 \\ c_{12} & c_{12} & c_{11} & 0 & 0 & 0 \\ 0 & 0 & 0 & c_{44} & 0 & 0 \\ 0 & 0 & 0 & 0 & c_{44} & 0 \\ 0 & 0 & 0 & 0 & 0 & c_{44} \end{bmatrix} \tag{68}$$

$$c_{12} = c_{11} - 2c_{44} \tag{69}$$

Substituting these two parameters into the acoustic wave equations (66) and (67) gives the field equations for isotropic elastic media that are presented in matrix form as:

$$\begin{bmatrix} \partial T_1 / \partial x + \partial T_5 / \partial z + \partial T_6 / \partial y \\ \partial T_2 / \partial y + \partial T_4 / \partial z + \partial T_6 / \partial x \\ \partial T_3 / \partial z + \partial T_4 / \partial y + \partial T_5 / \partial x \end{bmatrix} = \rho \partial / \partial t \begin{bmatrix} v_1 \\ v_2 \\ v_3 \end{bmatrix} \tag{70}$$

$$\begin{bmatrix} c_{11}\partial v_1/\partial x + c_{12}\partial v_2/\partial y + c_{12}\partial v_3/\partial z \\ c_{12}\partial v_1/\partial x + c_{11}\partial v_2/\partial y + c_{11}\partial v_3/\partial z \\ c_{12}\partial v_1/\partial x + c_{12}\partial v_2/\partial y + c_{11}\partial v_3/\partial z \\ c_{44}\partial v_2/\partial z + c_{44}\partial v_3/\partial y \\ c_{44}\partial v_1/\partial z + c_{44}\partial v_3/\partial y \\ c_{44}\partial v_1/\partial y + c_{44}\partial v_2/\partial x \end{bmatrix} = \partial/\partial t \begin{bmatrix} T_1 \\ T_2 \\ T_3 \\ T_4 \\ T_5 \\ T_6 \end{bmatrix} \tag{71}$$

To illustrate the FDTD technique for acoustic wave propagation, a 2-D elastodynamics problem with $\partial/\partial y = 0$ is used. The 3-D field equations (70) and (71) transform into 2-D equations (72) and (73), by setting all of the partial derivatives with respect to y to zero.

$$\begin{bmatrix} \partial T_1/\partial x + \partial T_5/\partial z \\ \partial T_4/\partial z + \partial T_6/\partial x \\ \partial T_3/\partial z + \partial T_5/\partial x \end{bmatrix} = \rho\partial/\partial t \begin{bmatrix} v_1 \\ v_2 \\ v_3 \end{bmatrix} \tag{72}$$

$$\begin{bmatrix} c_{11}\partial v_1/\partial x + c_{12}\partial v_3/\partial z \\ c_{12}\partial v_1/\partial x + c_{11}\partial v_3/\partial z \\ c_{12}\partial v_1/\partial x + c_{11}\partial v_3/\partial z \\ c_{44}\partial v_2/\partial z \\ c_{44}\partial v_1/\partial z + c_{44}\partial v_3/\partial x \\ c_{44}\partial v_2/\partial x \end{bmatrix} = \partial/\partial t \begin{bmatrix} T_1 \\ T_2 \\ T_3 \\ T_4 \\ T_5 \\ T_6 \end{bmatrix} \tag{73}$$

Before applying the FDTD technique, a key observation is made about these field equations. Equations (72) and (73) can be categorized into two groups based on their field interdependency in a manner similar to EM modes. The first group is formed using the fields T_1, T_3, T_5 & v_1, v_3, and the second group is created using the fields T_2, T_4, T_6 & v_2. It is noted that the second group does not influence the first group; therefore, each groups

is independent of each other. For rest of the analysis we only use the first group to simulate the electrodynamic problem.

The FDTD algorithm can be applied to these elastic wave equations using the leap frog method, along with a grid cell that is similar to Yee's, as shown in Fig. 11. This cell has fields cleverly spaced to satisfy the spatial differencing of the isotropic elastic media.

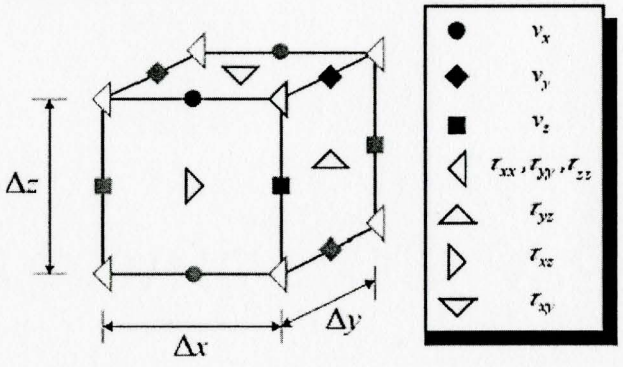

Figure 11: Grid Cell for Isotropic Elastic Media [9].

The first group is then discretized using the FDTD method with uniform cell sizes.

$$v_{1\,i,j}^{\,n+1} = v_{1\,i,j}^{\,n} + \frac{\Delta t}{\rho \Delta x}\left(T_{1i+.5,j}^{n+.5} - T_{1i-.5,j}^{n+.5} + T_{5i,j+.5}^{n+.5} - T_{5i,j-.5}^{n+.5}\right) \tag{74}$$

$$v_{3\,i+.5,j+.5}^{\,n+1} = v_{3\,i+.5,j+.5}^{\,n} + \frac{\Delta t}{\rho \Delta x}\left(T_{5i+1,j+.5}^{n+.5} - T_{5i,j+.5}^{n+.5} + T_{3i+.5,j+1}^{n+.5} - T_{3i+.5,j}^{n+.5}\right) \tag{75}$$

$$T_{1\,i+.5,j}^{\,n+.5} = T_{1\,i+.5,j}^{\,n-.5} + \frac{\Delta t}{\Delta x}\left(c_{11}\left\{v_{1i+1,j}^{n} - v_{1i,j}^{n}\right\} + c_{12}\left\{v_{3i+.5,j+.5}^{n} - v_{3i+.5,j-.5}^{n}\right\}\right) \tag{76}$$

$$T_{3\,i+.5,j}^{\,n+.5} = T_{3\,i+.5,j}^{\,n-.5} + \frac{\Delta t}{\Delta x}\left(c_{12}\left\{v_{1i+1,j}^{n} - v_{1i,j}^{n}\right\} + c_{11}\left\{v_{3i+.5,j+.5}^{n} - v_{3i+.5,j-.5}^{n}\right\}\right) \tag{77}$$

$$T_{5\,i,j+.5}^{\,n+.5} = T_{5\,i,j+.5}^{\,n-.5} + \frac{\Delta t}{\Delta x}\left(c_{44}\left\{v_{3i+.5,j+.5}^{\,n} - v_{3i-.5,j+.5}^{\,n}\right\} + c_{44}\left\{v_{1i,j+1}^{\,n} - v_{1i,j}^{\,n}\right\}\right) \tag{78}$$

The FDTD technique for elastic media also faces the same stability criterion as the FDTD method applied to EM. This criterion states that the time step must be less than or equal to the ratio of the grid cell size over the phase velocity. However, unlike EM, there is more than one velocity to consider. The velocity that is used is the one that results in the smallest time step. Since phase velocity is inversely proportional to the time step, the largest velocity has to be used. For acoustic waves, the largest phase velocity is the longitudinal velocity. The Courant criterion with same grid size in all three dimensions is stated below. This criterion is dependent on the number of dimensions of the simulated space.

$$1-D \Rightarrow \Delta t \le \frac{\Delta x}{v_{\max}\sqrt{1}} \tag{79}$$

$$2-D \Rightarrow \Delta t \le \frac{\Delta x}{v_{\max}\sqrt{2}} \tag{80}$$

$$3-D \Rightarrow \Delta t \le \frac{\Delta x}{v_{\max}\sqrt{3}} \tag{81}$$

Fig. 12 presents some snapshots of the particle velocities and stress fields. The wave is excited using particle velocity one, with a hard source placed at the centre of the computational domain.

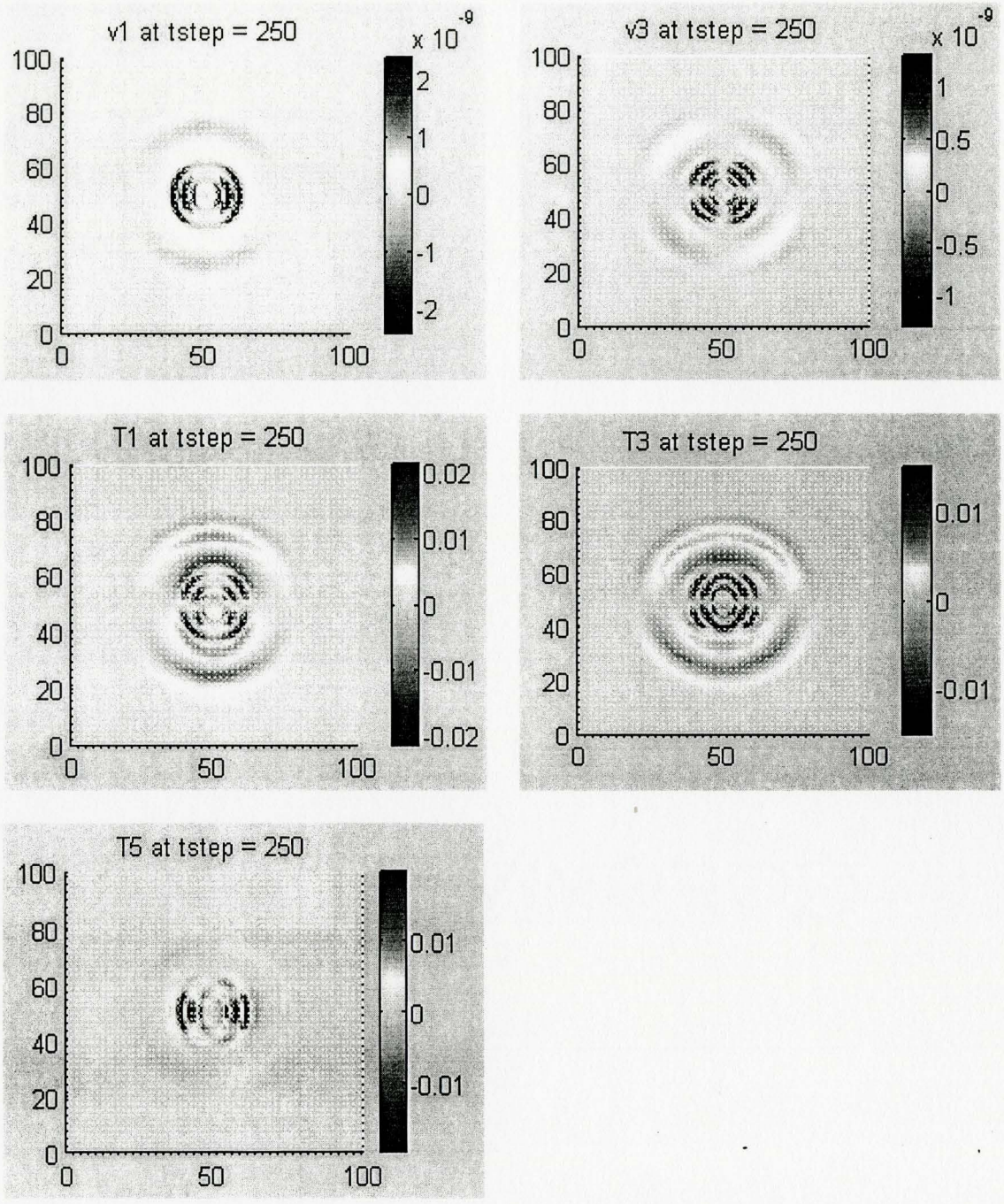

Figure 12: Snapshots of Elastic Wave fields for isotropic media.

After successfully applying the FDTD technique to isotropic media, the next natural step is to extend this technique to simulate anisotropic media. The following section presents details of this implementation.

4.4. FDTD applied to Piezoelectrics

Wave propagation in the piezoelectric media is described by a sophisticated and unique combination of acoustic and electromagnetic fields. The piezoelectric equations presented in Chapter 2 are developed under the quasi-static assumption for the electromagnetic fields. This assumption provides the capability to focus on only the acoustic wave propagation aspect while taking the piezoelectricity into account. The reason for using the quasi-static approximation has much to do with the FDTD technique. The problem arises from the Courant stability criterion that requires the time step to be inversely proportional to the largest phase velocity in the media. For the piezoelectric media, this is the speed of light. Since the velocity for the acoustic wave is five orders of magnitude smaller than the speed of light, the time step is too small an increment to see any acoustic wave propagate. The solution to this stalemate situation is to introduce the quasi-static assumption for EM fields in the following set of piezoelectric equations expressed in equations (82) to (85) [2].

$$\nabla \times \mathbf{E} = -\frac{\partial \mathbf{B}}{\partial t} = -\boldsymbol{\mu}\frac{\partial \mathbf{H}}{\partial t} \tag{82}$$

$$\nabla \times \mathbf{H} = \frac{\partial \mathbf{D}}{\partial t} = \frac{\partial}{\partial t}\left(\boldsymbol{\varepsilon}^{\mathrm{T}}\mathbf{E} + \mathbf{d}\mathbf{T}\right) \tag{83}$$

$$\nabla_s \mathbf{v} = \frac{\partial \mathbf{S}}{\partial t} = \frac{\partial}{\partial t}\left(\mathbf{d}^{t}\mathbf{E} + \mathbf{s}^{E}\mathbf{T}\right) \tag{84}$$

$$\nabla \cdot \mathbf{T} = \rho \frac{\partial \mathbf{v}}{\partial t} \tag{85}$$

where

B is the magnetic flux density vector

d is the (3 x 6) piezoelectric strain coefficient matrix

D is the electric flux density vector

E is the electric field vector

$\boldsymbol{\varepsilon}^{T}$ is the (3 x 3) electric permittivity matrix

H is the magnetic field vector

$\boldsymbol{\mu}$ is the (3 x 3) magnetic permeability matrix

$\mathbf{s}^{E}$ is the compliance coefficient matrix & is equivalent to inverse of the stiffness matrix

S is the strain vector

T is the stress vector

ρ is the diagonal (3 x 3) material density matrix

v is the particle velocity vector.

For the quasi-static approximation we assume the EM fields to be constant for the piezoelectric simulation analysis. This approximation allows changing the curl of H and the curl of E to be zero since electric field components are assumed to be static. The effect is that equation (82) becomes zero while the other three equations become

$$0 = \frac{\partial}{\partial t}\left(\boldsymbol{\varepsilon}^{\mathrm{T}}\mathbf{E} + \mathbf{d}\mathbf{T}\right) \tag{86}$$

$$\nabla_s \mathbf{v} = \frac{\partial}{\partial t}\left(\mathbf{d}'\mathbf{E} + \mathbf{s}^{\mathbf{E}}\mathbf{T}\right) \tag{87}$$

$$\nabla \cdot \mathbf{T} = \rho \frac{\partial \mathbf{v}}{\partial t} \tag{88}$$

Further simplification to these equations can be made with an introduction of a new constant, the piezoelectric stiffened compliance, equated below [2].

$$\hat{\mathbf{s}}^{\mathbf{E}} = \mathbf{s}^{\mathbf{E}} - \mathbf{d}'\left(\boldsymbol{\varepsilon}^{\mathrm{T}}\right)^{-1}\mathbf{d} \tag{89}$$

When this new constant is substituted into equation (87), it simplifies into equation (90).

$$\nabla_s \mathbf{v} = \hat{\mathbf{s}}^{\mathbf{E}} \frac{\partial \mathbf{T}}{\partial t} \tag{90}$$

Since the compliance matrix is equivalent to inverse of the stiffness matrix, then the inverse can be substituted into equation (90), resulting in the two piezoelectric field equations (91) and (92).

$$\nabla \cdot \mathbf{T} = \rho \frac{\partial \mathbf{v}}{\partial t} \tag{91}$$

$$\hat{\mathbf{c}}^{\mathbf{E}} \nabla_s \mathbf{v} = \frac{\partial \mathbf{T}}{\partial t} \tag{92}$$

These equations are the same as those derived in Chapter 2 for the piezoelectric equation analysis.

To discretize these equations, first the computational domain must be divided into grid cells. In the case of EM, Yee's cell, shown in Fig. 8, was used. In the case of isotropic elastic wave propagation, the grid cell, shown in Fig. 11, was used. Both of these cells are novel designs made specifically to discretize the field equations. For the piezoelectrics, various choices of grid cells can be used, other than that used for isotropic elastic media.

One available choice of grid cell is shown in Fig. 13 [3]. This figure shows the type of organization of fields in a cell that is known as unstaggered. All stress field components are placed at one point of the cell, and all velocity components are located one space interval away from the stress fields. The second type of available grid cell is the staggered and collocated cell, depicted in Fig. 14. This grid has all stress fields at one point, and all velocity components are half-space intervals away in both x and y directions, in turn requiring the averaging of the neighboring field components when performing central differencing.

For example, computing the new stress value at i,j requires computing a difference of velocity components at i+.5,j and i-.5,j. However, velocity values at those locations are not available due to the grid cell design. Hence, an average of the velocity at i+.5,j+.5 and i+.5,j-.5 must be computed for a velocity value required at i+.5,j.

Similarly, an average of the velocity at i-.5,j-.5 and i-.5,j+.5 must be computed to obtain a velocity value at i-.5,j. Hence, using the grid cell in Fig. 14 requires the averaging operation of the neighboring field values to perform the central differencing of field equations.

Neither of these two grids cells has the clever design that the isotropic elastic grid cell shown in Fig, 11 has. These two grid cells do not place field components based on its field differencing. For instance, the grid cell in Fig. 11 places T_1 across v_1 spaced out in x direction so as to satisfy the new velocity to be calculated by equation (74). Similarly, it places T_5 over and above v_1, in z direction, to satisfy the z differencing of T_5 that the new v_1 needs in equation (74). For this reason, Fig. 11 supersedes the other two grids, which can be used to spatially discretize the piezoelectric computation.

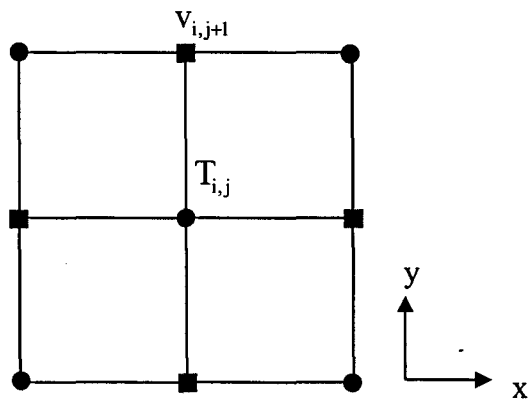

Figure 13: Unstaggered collocated grid.

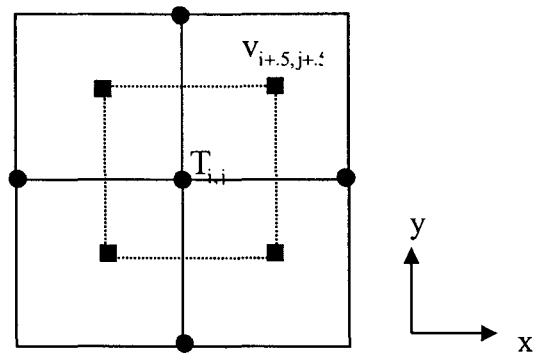

Figure 14: Staggered collocated grid.

Therefore the piezoelectric equations can then be discretized using the grid cell for isotropic elastic media (provided in Fig. 11), using the leap frog method. The piezoelectric material used for demonstrating acoustic waves is Bismuth Germanium Oxide ($Bi_{12}GeO_{20}$). This cubic material's elastic constant matrix is given in equation (93) and is conditioned using equation (89), which is then inversed so that it could be used in piezoelectric wave simulation.

$$\begin{bmatrix} c_{11} & c_{12} & c_{12} & 0 & 0 & 0 \\ c_{12} & c_{11} & c_{12} & 0 & 0 & 0 \\ c_{12} & c_{12} & c_{11} & 0 & 0 & 0 \\ 0 & 0 & 0 & c_{44} & 0 & 0 \\ 0 & 0 & 0 & 0 & c_{44} & 0 \\ 0 & 0 & 0 & 0 & 0 & c_{44} \end{bmatrix} \tag{93}$$

The location of the elements of equation (93) remains the same after conditioning this matrix. These elements are in a position identical to those elements for isotropic media. The only difference is that the isotropy condition does not have to be satisfied. Therefore, the cubic system has three independent constants, whereas isotropic media has

two. The discretization procedure of the FDTD technique for the cubic piezoelectric media is the same as that for the isotropic elastic media. Following these steps, the simulation is carried out. Snapshots of it are shown in Fig. 15.

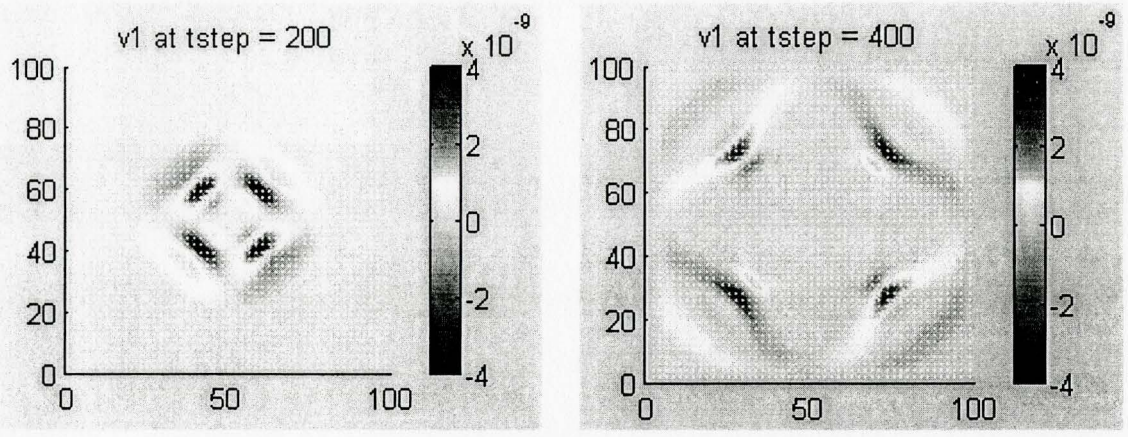

Figure 15: FDTD simulation of cubic piezoelectric crystal name Bismuth Germanium Oxide.

Successful implementation of the FDTD algorithm in all three media has enriched the world of numerical simulation with an advanced technique to numerically solve partial differential equations for waves. The next step is to solve open boundary problems, which are without any physical boundary conditions, to allow infinite media to be emulated. Such emulation is often required to simulate various devices. The following chapter looks into this problem and its solution for all three media.

Chapter 5

5. Perfectly Matched Layer

5.1. Introduction

The wave phenomenon faces boundary conditions that provide a unique solution to its partial differential equations. Sometimes it is necessary to simulate open regions that are without boundary conditions and so they require unlimited computational resources. To solve this problem, the wave must be absorbed at the boundary of a finite computational domain. Over the last three decades, much research has sought to find a suitable absorbing boundary condition (ABC) in an effort to simulate infinite media.

Much of the research to find an ABC started in the 1970s. Some of the famous boundary conditions developed at that time were the "radiation boundary" by D. Merewether and a "matched layer" by J. P. Berenger [4]. Even for the acoustic waves, a one-way approximation technique was made available by Engquist and Majda. The limiting factor of these ABCs is that they are effective only if the wave propagates perpendicularly to the boundary. Hence, the research to find a suitable ABC continued until 1994 when J. P. Berenger introduced an ABC that absorbed any plane wave that traveled with an arbitrary incident angle [3, 7]. His design involved a layer that is perfectly matched with the simulation media, resulting in a reflectionless layer that effectively absorbs the incoming wave.

Since the introduction of this Perfectly Matched Layer (PML), vigorous efforts have been put forth to simulate open regions in EM and in acoustics. In this chapter, details of Berenger's PML in EM are presented, followed by a discussion of its use in an elastic media and its development for the piezoelectrics.

5.2. PML in EM

Various applications in EM, such as waveguides or antennas, need an open region simulation. The advancement of the FDTD technique by the development of the PML enables such devices to be simulated. The PML is essentially an absorbing layer that is matched to a simulation media so as to eliminate any reflections that the interface may introduce.

A 2-D TEz mode is used to explain how to design the PML. The equations in free space are:

$$\varepsilon_o \frac{\partial E_x}{\partial t} + \sigma_e E_x = \frac{\partial H_z}{\partial y} \tag{94}$$

$$\varepsilon_o \frac{\partial E_y}{\partial t} + \sigma_e E_y = \frac{\partial H_z}{\partial x} \tag{95}$$

$$\mu \frac{\partial H_z}{\partial t} + \sigma_m H_z = -\left(\frac{\partial E_y}{\partial x} + \frac{\partial E_x}{\partial y} \right) \tag{96}$$

The layer's main focus is to decay any wave components that are normal to the boundary interface. With this purpose in mind, the field equations within the PML region are split according to their spatial derivatives. For instance, equation (96) is separated using the H_z field, which is split according to its spatial derivatives x and z. The two new fields are H_z^x and H_z^y, which result in equations (99) and (100).

$$\varepsilon_o \frac{\partial E_x}{\partial t} + \sigma_e^y E_x = \frac{\partial (H_z^x + H_z^y)}{\partial y} \tag{97}$$

$$\varepsilon_o \frac{\partial E_y}{\partial t} + \sigma_e^x E_y = -\frac{\partial (H_z^x + H_z^y)}{\partial x} \tag{98}$$

$$\mu \frac{\partial H_z^x}{\partial t} + \sigma_m^x H_z^x = -\left(\frac{\partial E_y}{\partial x} \right) \tag{99}$$

$$\mu \frac{\partial H_z^y}{\partial t} + \sigma_m^y H_z^y = \frac{\partial E_x}{\partial y} \tag{100}$$

The split field equations transform into the Maxwell's equations for vacuum when $\sigma_e^x = \sigma_e^y = 0$ and $\sigma_m^x = \sigma_m^y = 0$. If $\sigma_m^x = \sigma_m^y = 0$ and $\sigma_e^x = \sigma_e^y = \sigma_e$, then these equations represent an electrically conductive medium. An absorbing layer is produced when material parameters of both regions satisfy the equalities $\mu_2 = \mu_1$, $\varepsilon_2 = \varepsilon_1$, $\sigma_m^x = \sigma_m^y = \sigma_m$, $\sigma_e^x = \sigma_e^y = \sigma_e$ [3, 7].

Now, to absorb only the normal wave components (e.g., in the x direction), the absorbing layer imposes $\sigma_e^y = \sigma_m^y = 0$. This condition provides a layer that absorbs plane

waves traveling in the x direction (e.g., the fields E_y, H_z^x for the TEz mode). At the same time, the layer does not absorb any fields that are traveling in the y direction (e.g., E_x, H_z^y). Similarly, when $\sigma_e^x = \sigma_m^x = 0$ is applied, the fields E_x, H_z^y are absorbed while the fields E_y, H_z^x are not. These are the properties of Berenger's PML that result in the absorbing layer. Fig. 16 shows further details on how to use the attenuation parameters to implement the PML for EM. It is noteworthy that at the corner regions both attenuation constants are non-zero [3].

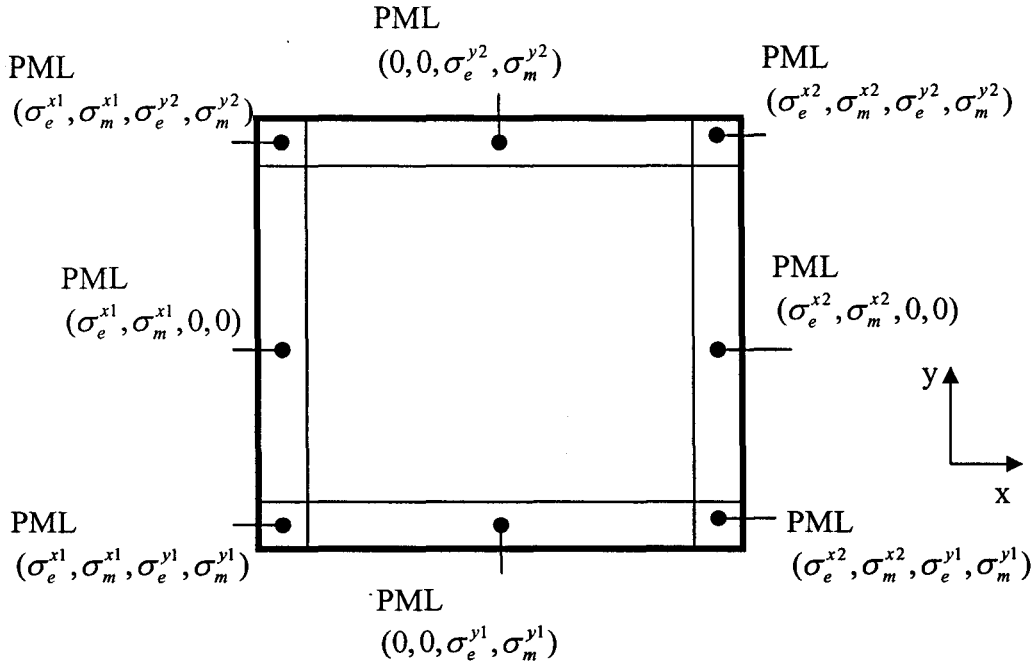

Figure 16: Perfectly Matched Layer surrounding the computational domain [7].

The layer's attenuation parameters are designed to absorb any incoming wave; however, to be reflectionless the layer must also be matched. The idea of matching layer comes from the microwave theory of impedance matching. When a traveling wave faces a change in the medium, the second medium must have the same impedance as the first to

avoid reflecting any part of the incoming wave. Thus, designing a reflectionless layer requires impedance matching for the EM case.

The reflection coefficient for a normally incident wave is given in equation (101). To calculate the reflection coefficient requires impedance of two, medium one and medium two. Impedance of the first medium, which is vacuum, is given in equation (102) and impedance of the second medium, which is PML, is given in equation (103). When the two impedances are equal as equated in equation (104), the reflection coefficient equals zero, constructing a reflectionless layer. To make the two impedances equal, a necessary matching condition must be met. This condition is stated by equation (105).

$$\Gamma = \frac{\eta_1 - \eta_2}{\eta_1 + \eta_2} \tag{101}$$

$$\eta_1 = \sqrt{\frac{\mu_1}{\varepsilon_1}} \tag{102}$$

$$\eta_2 = \sqrt{\frac{\mu_2\left(1+\frac{\sigma_m}{j\omega\mu_2}\right)}{\varepsilon_2\left(1+\frac{\sigma_e}{j\omega\varepsilon_2}\right)}} \tag{103}$$

$$\sqrt{\frac{\mu_1}{\varepsilon_1}} = \sqrt{\frac{\mu_2\left(1+\frac{\sigma_m}{j\omega\mu_2}\right)}{\varepsilon_2\left(1+\frac{\sigma_e}{j\omega\varepsilon_2}\right)}} \tag{104}$$

$$\frac{\sigma_e}{\varepsilon_1} = \frac{\sigma_m}{\mu_1} \tag{105}$$

The analysis above is performed for a normal incident plane wave. A similar derivation reveals that the same matching condition is required to obtain a reflectionless interface for an oblique incident plane wave [3].

In theory, meeting this matching condition guarantees a reflectionless boundary; unfortunately, in practice this is not the case. Due to discretization of equations, numerical error is introduced. One error comes from the discontinuity of the attenuation parameters. This error can be minimized by making the attenuation factor large and as smooth as possible. This criterion is satisfied by attenuating exponentially. Some examples of the exponentially differenced FDTD equations within the PML region are given in equations (106) and (107).

$$E_{yi,j+.5}^{n+1} = e^{-\sigma_{ex(i)}\Delta t/\varepsilon_o} E_{yi,j+.5}^{n} - \frac{\left(1-e^{-\sigma_{ex(i)}\Delta t/\varepsilon_o}\right)}{\sigma_{ex(i)}\Delta x}\left[H_{z\,i+.5,j+.5}^{x\,n+.5} - H_{z\,i-.5,j+.5}^{x\,n+.5} + H_{z\,i+.5,j+.5}^{y\,n+.5} - H_{z\,i-.5,j+.5}^{y\,n+.5}\right] \quad (106)$$

$$H_{z\,i+.5,j+.5}^{x\,n+.5} = e^{-\sigma_{mx(i+.5)}\Delta t/\mu_o} H_{z\,i+.5,j+.5}^{x\,n-.5} - \frac{\left(1-e^{-\sigma_{mx(i+.5)}\Delta t/\varepsilon_o}\right)}{\sigma_{mx(i+.5)}\Delta x}\left[E_{yi+1,j+.5}^{n} - E_{yi,j+.5}^{n}\right] \quad (107)$$

These equations have attenuation parameters as a function of the distance into the interface over the total length of the PML region, as expressed in equation (108).

$$\sigma(\rho) = \sigma_o \left(\frac{\rho}{\delta} \right)^n \tag{108}$$

where

σ_o is a maximum attenuation constant

ρ is the current location into the PML

δ is the total depth of the PML

n is exponent of attenuation, decided arbitrarily.

The attenuation parameter requires the maximum attenuation constant that is determined using equation (109), details of which are further discussed in [3].

$$\sigma_o = -\frac{(n+1)\ln[R(0)]}{2\eta\delta} \tag{109}$$

where

$R(0)$ is a reflection factor

η is wave impedance.

Two other sources of error come from the practical implementation of the PML. The first source of error is that PML's length must be of a finite thickness. The second source is that it must be terminated with a boundary condition, which often tends to be a perfect electrical conductor (PEC). These two factors lead to some finite power reflected back from the PEC into the non-PML region. To evaluate this reflected wave, a reflection factor is formulated in [3] as

$$R(\theta) = e^{-2\eta\sigma_o \delta \cos\theta/(n+1)} \tag{110}$$

where θ is the incident angle of a plane wave that is impinging upon the PML interface [3]. The user designs this parameter in advance, based on a balancing act between the numerical discretization error and the theoretical reflection factor. In order to minimize the reflection factor, the maximum attenuation factor has to be as large as possible. However, by permitting it to be large, the localized discontinuity step of the attenuation factor introduces larger numerical discretization errors. From various optimizing experiments, a conclusion has been reached that for an optimal design the reflection factor is $R(0) \approx e^{-16}$ when the PML is of 10 cell thickness in length. This gives the maximum attenuation factor to be [3]

$$\sigma_o = -\frac{(n+1)\cdot(-16)}{\eta\Delta} \tag{111}$$

With these design parameters, a 2-D TEz mode is simulated, and the results are indicated in Fig. 17. For comparison, Fig. 18 presents the case when the simulation is performed without the PML.

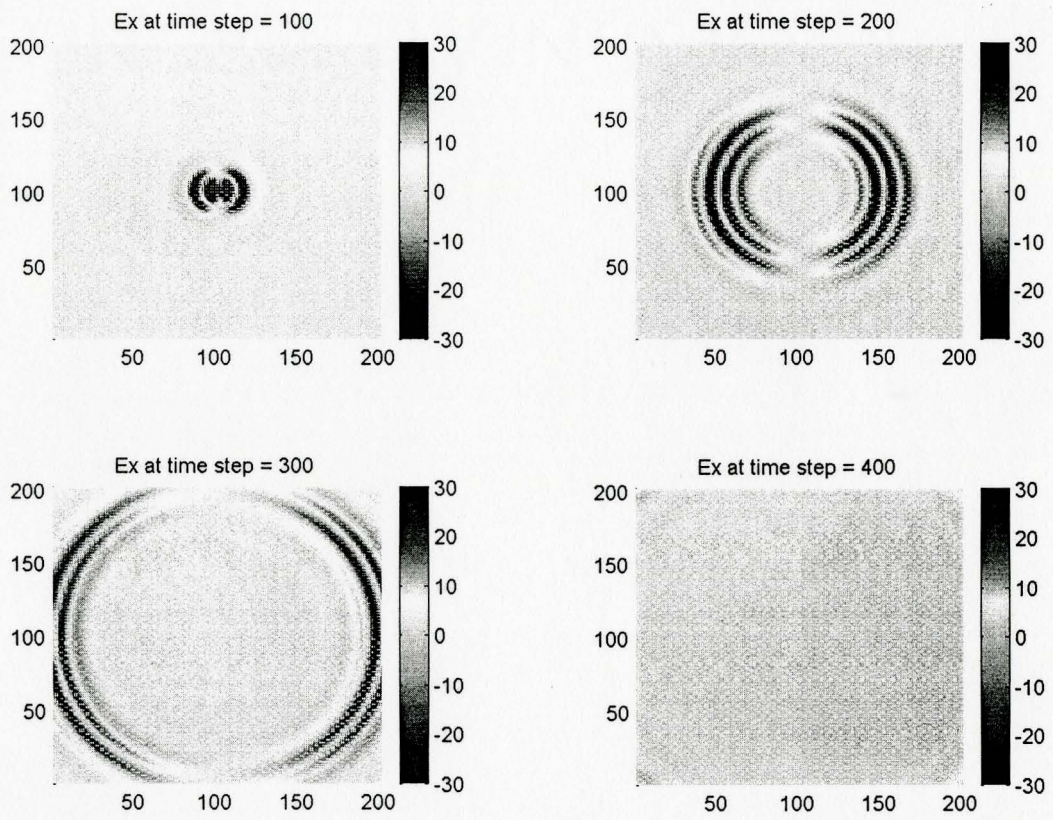

Figure 17: Ex of TEz mode simulated with the PML.

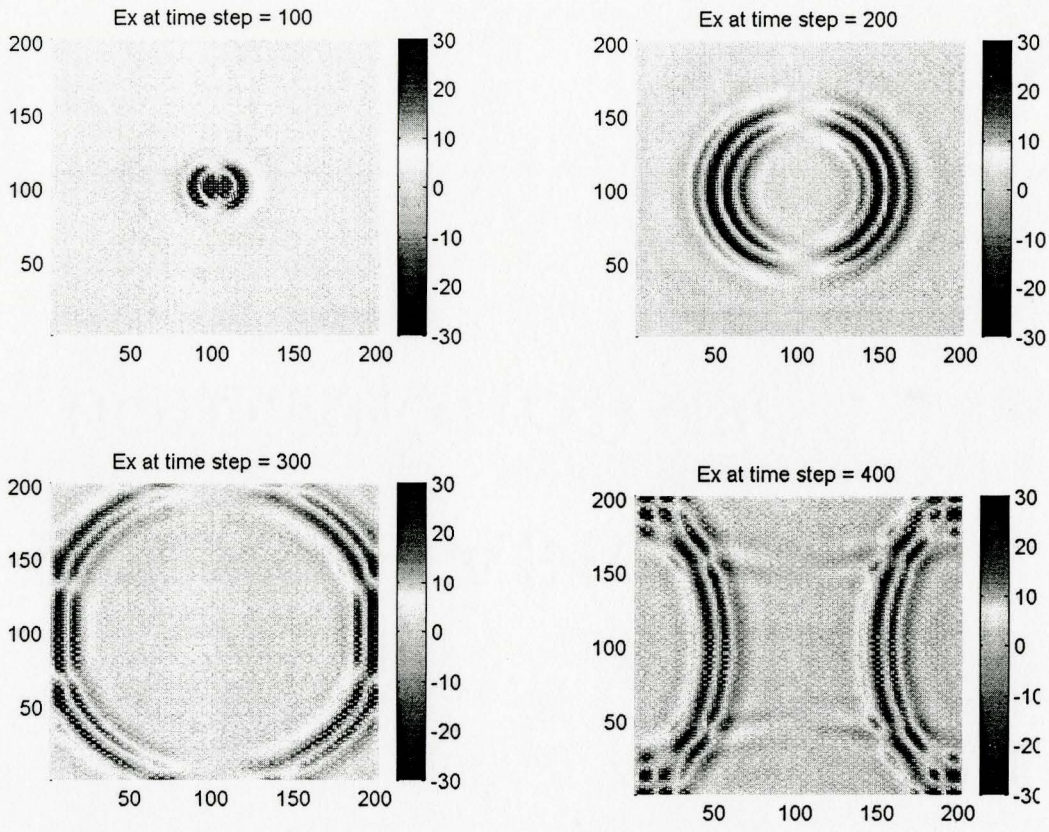

Figure 18: TEz mode simulated without the PML.

Snapshots of the electric field shown in Fig. 17 clearly demonstrate the absorption of the incoming wave. Due to practical considerations, some reflection does occur. A method to measure the effectiveness of the PML is therefore needed. A standard method developed to quantify the performance of the PML is by computation of the relative error.

This calculation is performed by comparing samples of a field from two different simulation domains. The first domain, which has the PML implemented, is simulated until the wave is fully absorbed. The second is simulated for the same amount of time as

the first domain but the grid is sized large enough to not face any reflections from the boundaries. This domain is called the reference domain since the samples obtained are without boundary errors.

The location of the test point is situated the same distance from the source for both simulation domains to ensure that the sample point is affected the same way by the propagating wave. Furthermore, to normalize the difference between the two domains, a maximum field value for the test point is measured in the reference domain over the course of the simulation.

Absolute value is taken for the difference between the samples and is then divided by the absolute value of the maxima of the wave at that location. Thus, the relative error is computed at every time step and is formulated in equation (112).

$$R\_err^{n}_{i,j} = \left| E^{n}_{i,j} - E^{n}_{ref\,i,j} \right| / \left| E_{ref\,\max i,j} \right| \qquad (112)$$

The relative error is reported to be less than 0.001% for a PML with the length of four grid cells. These results have outperformed any of the ABCs developed in EM thus far. As a result, the PML has become the standard ABC to be used.

Such extraordinary performance of an ABC has caught much attention of experts in other simulating media, such as elastic media. As a result, the PML has been developed in elastic media, the details of which are presented in the next section.

5.3. PML in Acoustics

The world of acoustic waves also had a dire need for an absorbing boundary condition able to give such marvelous performance as the PML. With the introduction of the PML in EM, much research has been geared towards its implementation in elastic media. The main idea behind Berenger's PML is to match the impedance of the layer to the simulation medium in order to get a reflectionless layer. This task proves to be difficult for an elastic media since they have two or three impedances to match.

In elastic media, the PML theory follows the same procedures as Berenger's PML. To absorb an incoming wave, acoustic field equations are separated into their parallel and normal components. Then the normal field components are attenuated within the PML. An example is a general acoustic wave, which equations (113) and (114) describe in terms of velocity with its initial condition.

$$\frac{\partial}{\partial t}\mathbf{v} - \mathbf{A}\frac{\partial}{\partial x}\mathbf{v} - \mathbf{B}\frac{\partial}{\partial y}\mathbf{v} = 0 \tag{113}$$

$$\mathbf{v}(t=0) = \mathbf{v}_o \tag{114}$$

where $\mathbf{v}$ is an m size vector; and $\mathbf{A}$, $\mathbf{B}$ are m x m matrices [4].

To construct a reflectionless layer, field equations are placed into two groups using parallel and normal criteria.

$$\frac{\partial}{\partial t}\mathbf{v}^{\parallel} - \mathbf{B}\frac{\partial}{\partial y}\mathbf{v} = 0 \tag{115}$$

$$\frac{\partial}{\partial t}\mathbf{v}^{\perp} - \mathbf{A}\frac{\partial}{\partial x}\mathbf{v} = 0 \tag{116}$$

Another wave u is introduced with a damping function d(x). This function is zero in the non-PML region and is applied to only the normal component of the wave, as described by equations (117) to (119).

$$\frac{\partial}{\partial t}\mathbf{u}^{\parallel} - \mathbf{B}\frac{\partial}{\partial y}\mathbf{u} = 0 \tag{117}$$

$$\frac{\partial}{\partial t}\mathbf{u}^{\perp} + d(x)\,\mathbf{u}^{\perp} - \mathbf{A}\frac{\partial}{\partial x}\mathbf{u} = 0 \tag{118}$$

$$\mathbf{u}(t=0) = \mathbf{v}_o \tag{119}$$

Since $\mathbf{u} \equiv \mathbf{v}$ in the non-PML region, it can be concluded that the model of the layer is perfectly matched and is reflectionless. A detailed plane wave analysis is derived to prove the reflectionless property in [4].

An example of an isotropic elastic wave in the PML region discretized by the FDTD technique is given by equations (120) and (121). These equations contain an attenuation parameter d(x), which is expressed in equation (122) [4].

$$v_1^{x\ n+1}_{i,j} = v_1^{x\ n}_{i,j}\left(\frac{2-\Delta td(x)_i}{2+\Delta td(x)_i}\right)+\frac{\Delta t}{\rho \Delta x}\left(\frac{2}{2+\Delta td(x)_i}\right)\left(T_1^{\ n+.5}_{i+.5,j}-T_1^{\ n+.5}_{i-.5,j}\right) \tag{120}$$

$$v_1^{z\ n+1}_{i,j} = v^{\ z^n}_{1\,i,j}\left(\frac{2-\Delta td(z)_j}{2+\Delta td(z)_j}\right)+\frac{\Delta t}{\rho \Delta z}\left(\frac{2}{2+\Delta td(z)_j}\right)\left(T_5^{\ n+.5}_{i,j+.5}-T_5^{\ n+.5}_{i,j-.5}\right) \tag{121}$$

$$d(x) = d_o\left(\frac{x}{\delta}\right)^2 \tag{122}$$

$$d_o = \log\left(\frac{1}{R}\right)\frac{3V_p}{2\delta} \tag{123}$$

Designing the attenuation parameter needs a few constants, such as the fastest phase velocity V_p, the maximum attenuation constant d_o, and the reflection factor R.

With these design parameters, the acoustic wave in an isotropic material is simulated. The results are revealed in Fig. 19. Fig. 20 depicts the situation in which the simulation domain is implemented without the PML. A comparison of these two figures indicates that the PML is working effectively.

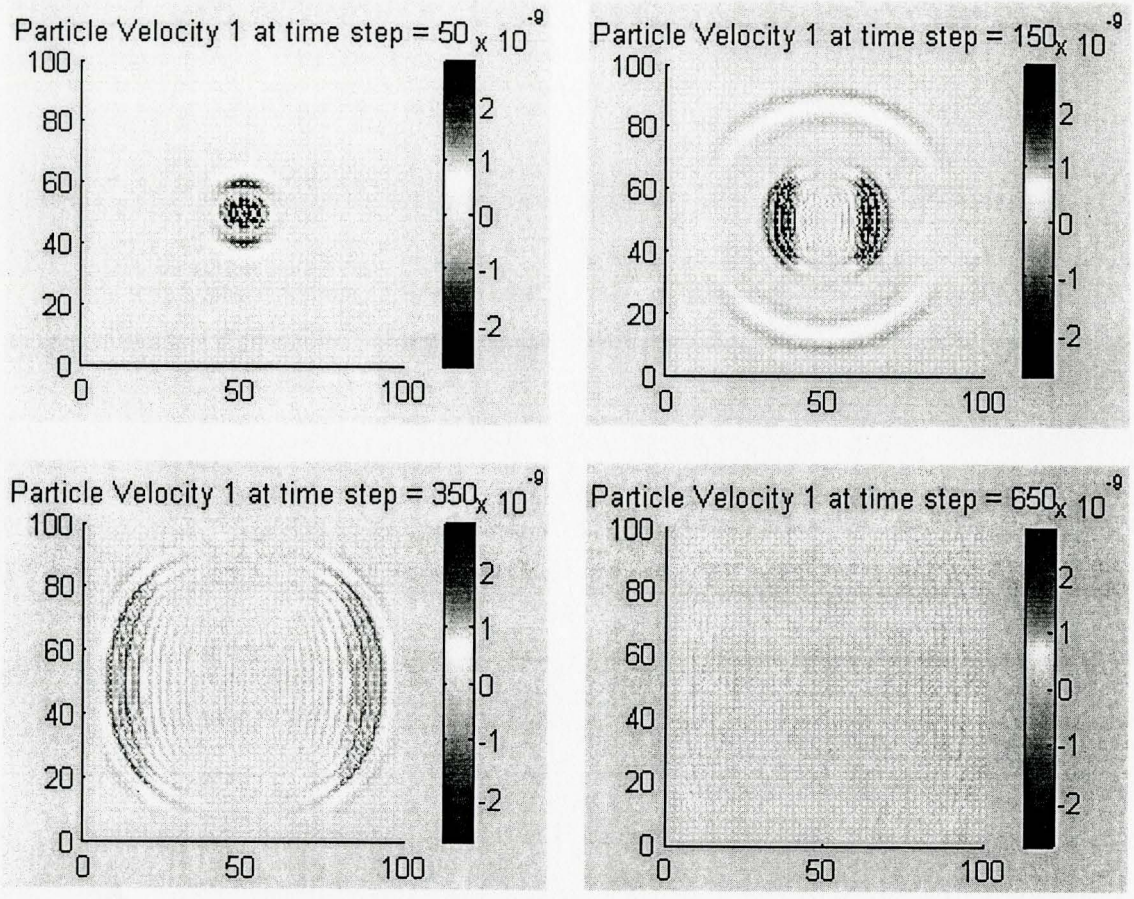

Figure 19: FDTD simulation of isotropic media with PML.

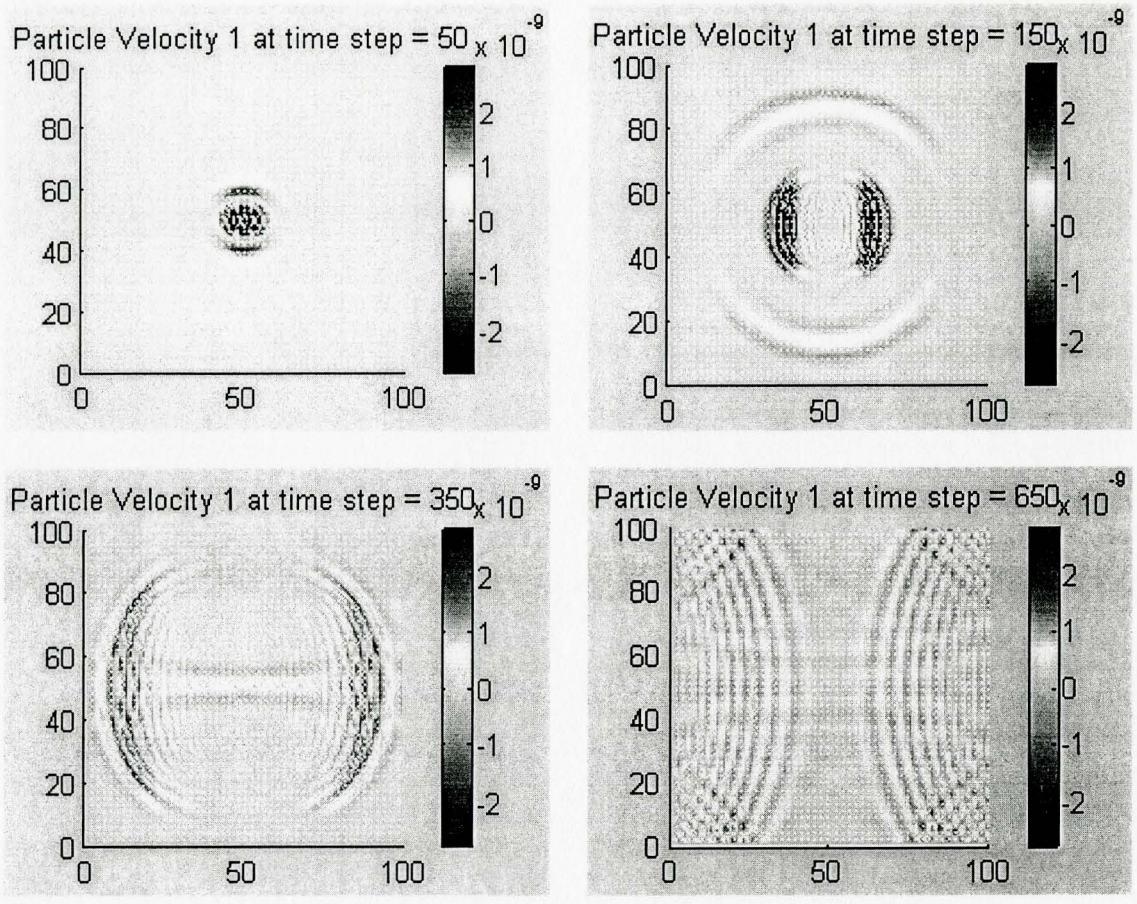

Figure 20: FDTD simulation of isotropic media without PML.

The acoustic PML faces reflection errors same as those in the electromagnetic case. Due to the finite thickness of the PML and the outer boundary conditions, there are reflections of approximately 0.1%. This efficiency is significantly better than any other ABC applied to isotropic elastic waves, thus making PML a standard ABC for elastic media [4].

The successful implementations of the PML, in conjunction with its outstanding performance in elastic media, lead to the possibility of extending the implementation to

anisotropic media. The next section discusses the details of implementing the PML in anisotropic media, specifically in piezoelectric media.

5.4. PML in Piezoelectrics

Many absorbing boundary conditions have been developed to simulate infinite media, although none have been demonstrated for piezoelectric crystals. The ABC introduced by Majda and Engquist can be applied to piezoelectrics, but it requires the wave to be normally incident for it to be effective [4].

F. Chagla and P. Smith were the first to apply PML in FDTD to simulate piezoelectric crystals. This implementation involves splitting the piezoelectric equations in the PML region into their normal and tangential components. Also, it requires adding attenuation to these piezoelectric equations, one of which is presented in equations (123) and (124) as an example.

$$\frac{\partial v_1^x}{\partial t} + d^x v_1^x = \frac{1}{\rho}\frac{\partial T_1}{\partial x} \tag{124}$$

$$\frac{\partial v_1^z}{\partial t} + d^z v_1^z = \frac{1}{\rho}\frac{\partial T_5}{\partial z} \tag{125}$$

In order to discretize these equations, a grid cell for piezoelectric crystal is used, as shown in Fig. 21.

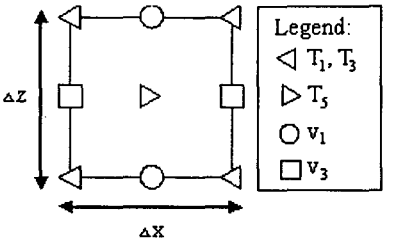

Figure 21: Grid cell for piezoelectric crystals.

Furthermore, to decay the incoming wave smoothly, the attenuation constants are introduced with explicit exponentially differencing. An example is given below:

$$
\begin{aligned}
v_1^x\,|_{i,j}^{n+1} &= \exp(-d_i^x \Delta t) v_1^x\,|_{i,j}^{n} + \\
&\quad \frac{1-\exp(-d_i^x \Delta t)}{d_i^x \rho \Delta x}\left(T_1\,|_{i+.5,j}^{n+.5} - T_1\,|_{i-.5,j}^{n+.5}\right) \\
v_1^z\,|_{i,j}^{n+1} &= \exp(-d_j^z \Delta t) v_1^z\,|_{i,j}^{n} + \\
&\quad \frac{1-\exp(-d_j^z \Delta t)}{d_j^z \rho \Delta z}\left(T_5\,|_{i,j+.5}^{n+.5} - T_5\,|_{i,j-.5}^{n+.5}\right)
\end{aligned}
\tag{126}
$$

where

$$d_i^x = d_o\left(\frac{x_i}{\zeta}\right)^2$$

$$d_i^z = d_o\left(\frac{z_i}{\zeta}\right)^2$$

$$\mathrm{d_o} = \log_e\left(\frac{1}{\mathrm{R}}\right)\frac{3\mathrm{V_p}}{2\zeta}$$

ζ is the finite PML thickness, R is the reflection coefficient, Δt is the time interval, and Δx, Δz are space intervals. The space intervals are set to $\lambda/20$, where λ is the wavelength of the highest frequency component in the simulation domain. The x-direction attenuation factor d^x is set to zero for fields that are in the z direction, while d^z

is set to zero for fields that are in the x direction, as shown in Fig. 22. At the four corner regions of the PML, both attenuation factors are non-zero. The rest of the velocities and stress equations are similarly discretized. When setting the time interval, the Courant stability criteria that must be satisfied is:

$$\Delta t \leq \frac{\Delta x}{v_{\max}\sqrt{2}} \tag{127}$$

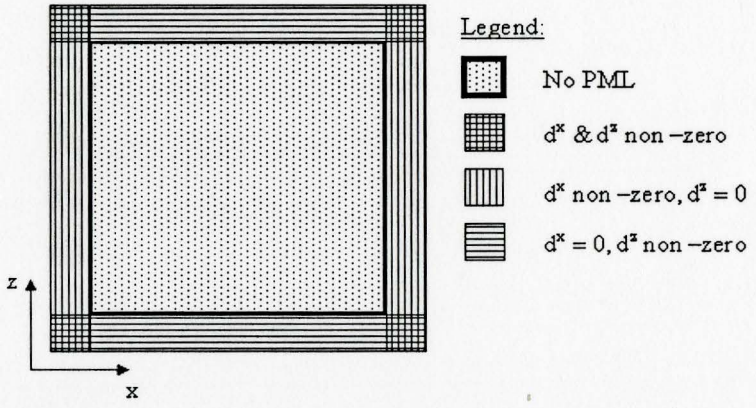

Figure 22: Implementation of attenuation constants.

Using the above derivations of the PML, a demonstration is prepared using a cubic piezoelectric material, Bismuth Germanium Oxide $Bi_{12}GeO_{20}$. This material has the longitudinal velocity of 3369.8 m/s when the Euler angle is <0, 0, 0>. Bismuth Germanium Oxide also has a material density of 9200 kg/m^3. The reflection coefficient R is set by trial and error to 5.335e-05. The two-dimensional computational domain contains 85 x 85 grid cells surrounded by a PML with the thickness of 7 cells on each side. One period of a 1 GHz sinusoidal signal is used as a point source at location (50, 50). The outer edge of the PML is assumed to be stress-free and immobile. The space

intervals are equal to 16.849 μm, while the time step size is set to 7.07 ps, which is five times smaller than required by the Courant condition, to give a smoother wave propagation display [1].

It takes 800 time steps for the wave to travel from the source location to the interface and be fully absorbed. The particle velocity v_1 ($v_1 = v_1^x + v_1^z$) is plotted in Figs. 23 and 24. Fig. 24 shows the problem of spurious reflections into the computational domain when the PML is not imposed. Fig. 23 demonstrates the successful implementation of the PML by showing snapshots of particle velocity v_1.

Piezoelectric media also faces the same reflection errors as those in EM. Due to the finite thickness of the PML and the outer boundary condition, some reflection of the wave does travel back into the non-PML domain. These residual reflections can be seen when the simulation domain is amplified by a factor of 50, as Fig. 25 indicates. A standard method of measuring reflection error comes from the PML theory in EM, which is the relative error stated in equation (128) [3]:

$$\varepsilon_r\big|_{i,j}^n = \frac{\left|\,|v_1|_{i,j}^n - v_{1\,ref}\big|_{i,j}^n\,\right|}{\left|\,v_{1\,ref\,\max}\big|_{i,j}^n\,\right|} \tag{128}$$

Table 2 presents the maximum value of this error is measured over the computational domain for various time steps. For the piezoelectric media, it is noted to be less than 0.5% [1].

This performance is highly acceptable in comparison to other ABC for anisotropic media. However, the next two chapters discuss the few drawbacks observed during this research.

Time Steps	Maximum Relative Error (%)
100	0.00606
200	0.04932
300	0.09651
400	0.13292
500	0.08278
600	0.21213
700	0.20979
800	0.20094
900	0.24353
1000	0.25538

Table 2: Maximum Reflection Error (%) for various time step, as the v_1 propagates from source to PML.

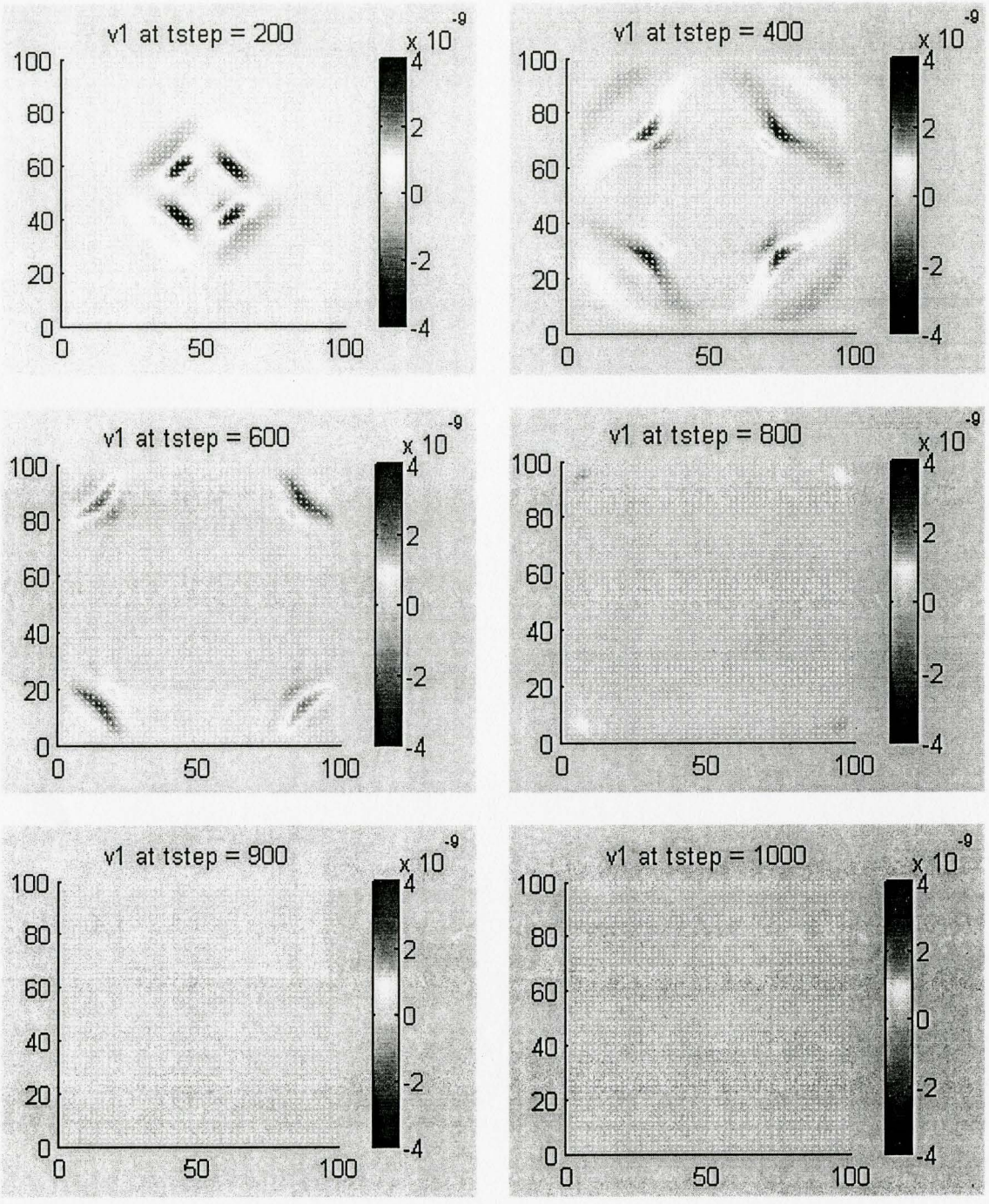

Figure 23: Snapshots of the particle velocity v_1.

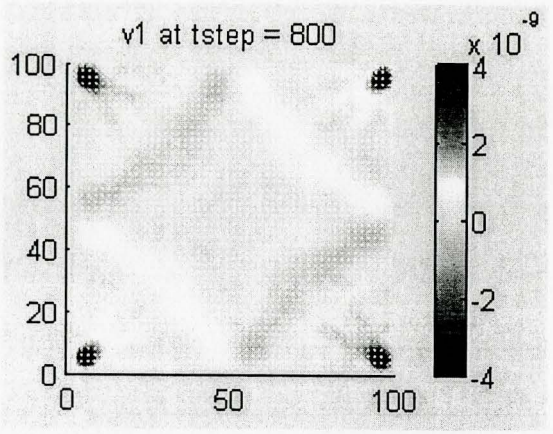

Figure 24: v_1 without PML at time step 800.

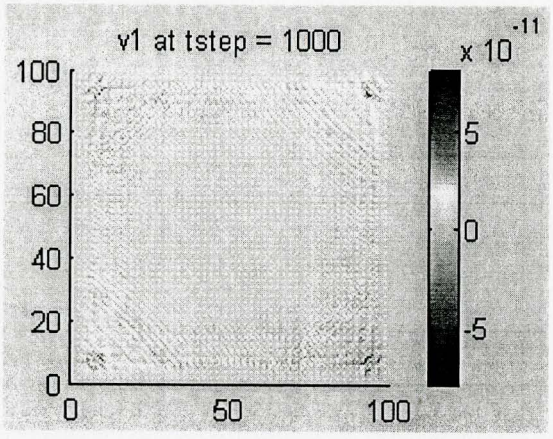

Figure 25: Zoom x50 of v_1 with PML at time step 1000.

Chapter 6

6. Stability Considerations for PML in Piezoelectric

6.1. Introduction

Simulating open boundaries involves limiting the size of the grid; therefore, a suitable boundary condition must be chosen so that the computations do not introduce ghost reflections from the edges of the grid. The Perfectly Matched Layer (PML) is acknowledged to be the boundary condition that most efficiently eliminates the reflections in isotropic solids. The previous chapter extended the concept of the PML to piezoelectric crystals and showed that it can also be extremely effective for acoustic wave propagation in non-isotropic solids. However, it is observed that the PML can experience instabilities. This chapter presents several examples of FDTD simulations that are used to deduce the necessary conditions for stability.

6.2. Slowness Curves and Stability Criterion

The FDTD technique must satisfy the numerical Courant stability criterion that was introduced in the previous chapter. However, the notion of stability to be discussed in this chapter is not of a numerical nature but a theoretical one. Therefore, even after fulfilling the numerical stability criterion, the simulation is sometimes unstable [8].

Due to excellent performance of the PML, various types of piezoelectric material were simulated to ensure its effectiveness. During these experiments, it was observed that the PML can experience instabilities when it is applied to solids with polar slowness curves that contain concave sections. This exploding behavior is shown in Fig. 26 for Gallium Arsenide GaAs, which is a cubic piezoelectric material. The corresponding slowness curve is given in Fig. 27.

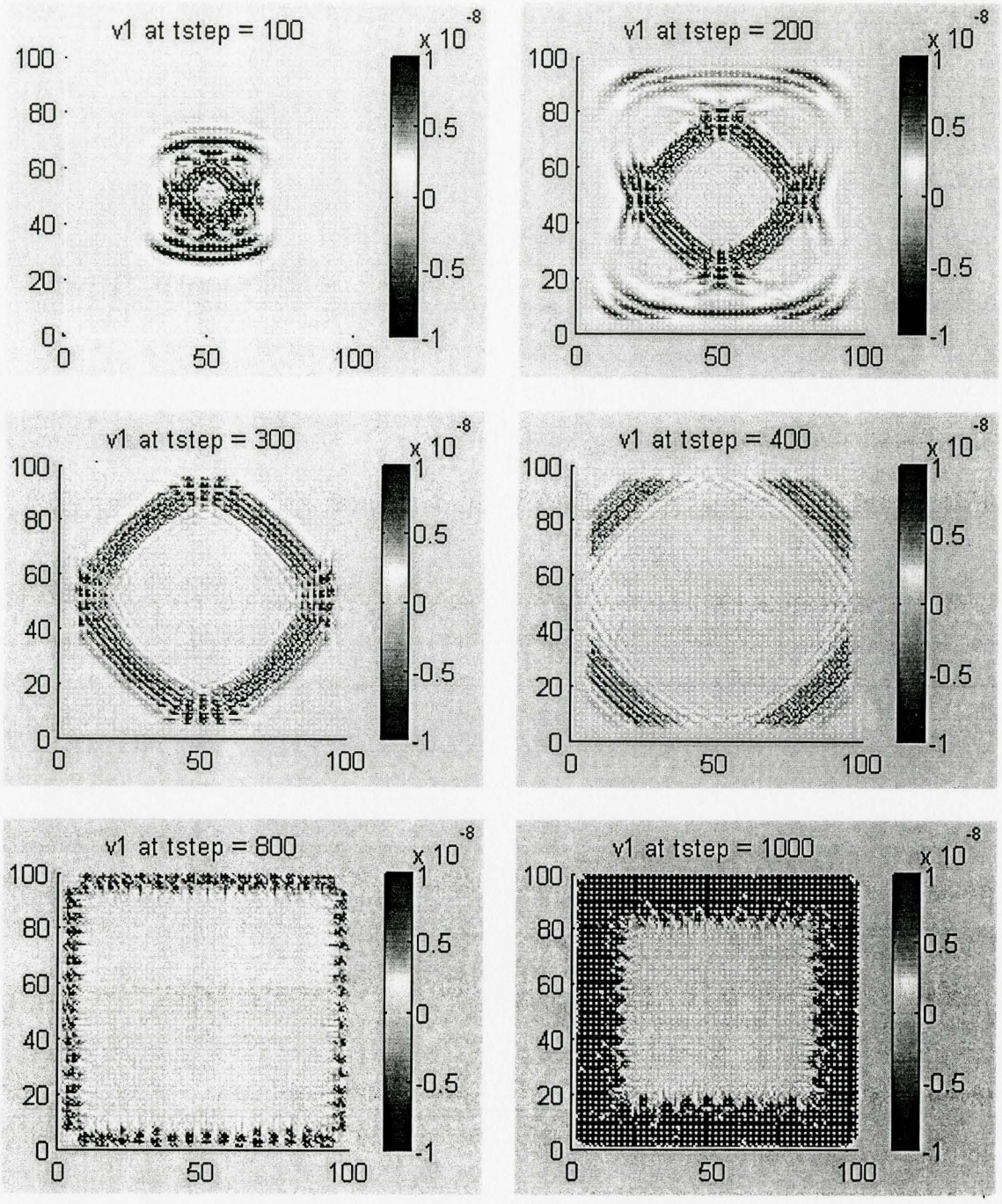

Figure 26: FDTD simulation of Gallium Arsenide with PML.

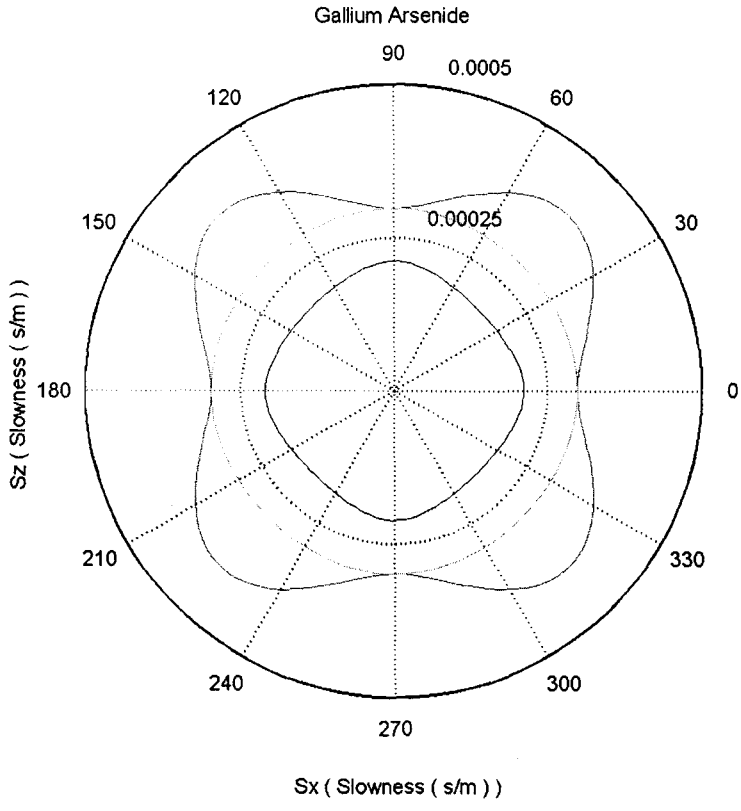

Figure 27: Slowness Curve of Gallium Arsenide.

This result does not imply that all materials with concave sections appearing in the slowness curves would result in an unstable PML. Bismuth Germanium Oxide has concaveness yet does not explode. In this experiment, the simulation is allowed to run 100,000 time steps to ensure stability. The simulation results presented in Fig. 28 show the wave being fully absorbed without exploding. The corresponding slowness curve with concaveness is depicted in Fig. 29.

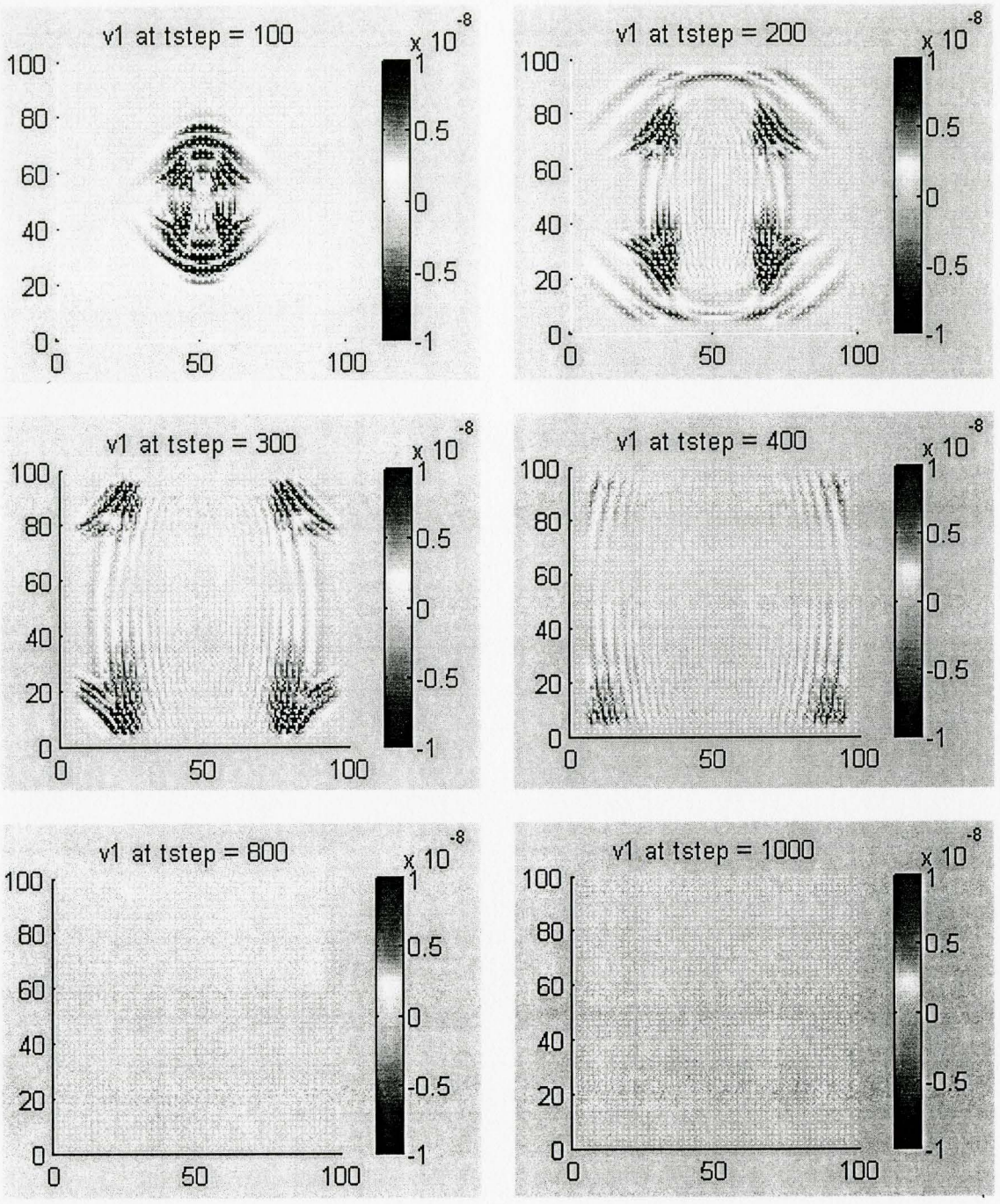

Figure 28: Snapshots of the particle velocity v_1 of Bismuth Germanium Oxide.

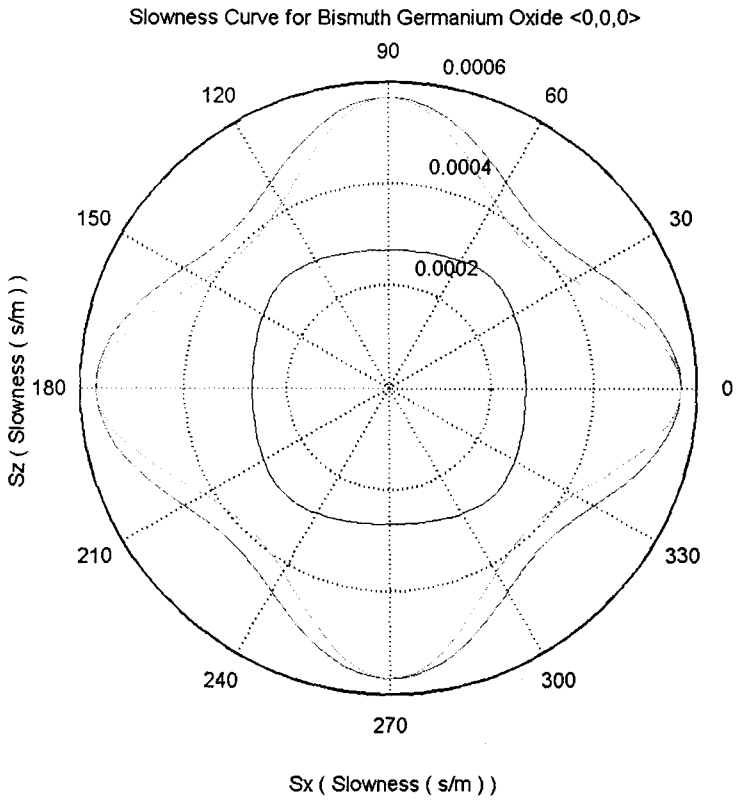

Figure 29: Slowness Curve for Bismuth Germanium Oxide.

It is important to comprehend why one material with concave section in slowness curve experiences instability while another material does not. Because of the relationship between slowness curve and group velocity, Bismuth Germanium Oxide does not explode. It is well known that group velocity describes energy flow propagation and is orthogonal to the slowness curve. To clarify the connection between the group velocity vectors and slowness vector, Fig. 30 illustrates the group velocity vector superimposed on a slowness curve along with its slowness vectors. At some areas of concaveness, the group velocity vector has one of its unit vectors in the opposite direction to its corresponding slowness vector. More specifically, in Fig. 30 the vertical component of the phase velocity vector is pointing in the positive direction, whereas the corresponding

vertical component of the group velocity vector is pointing in the negative direction. Hence, energy propagation is anti-parallel to the propagation vector. This phenomenon is known as the backward energy mode. When the wave enters the PML region in this mode, instead of starting to attenuate it actually begins to increase, resulting in instability of the PML. GaAs does not explode because it does not have a backward energy mode, as one can verify by following its slowness curve. The concave sections are the areas where the backward energy phenomenon usually occurs.

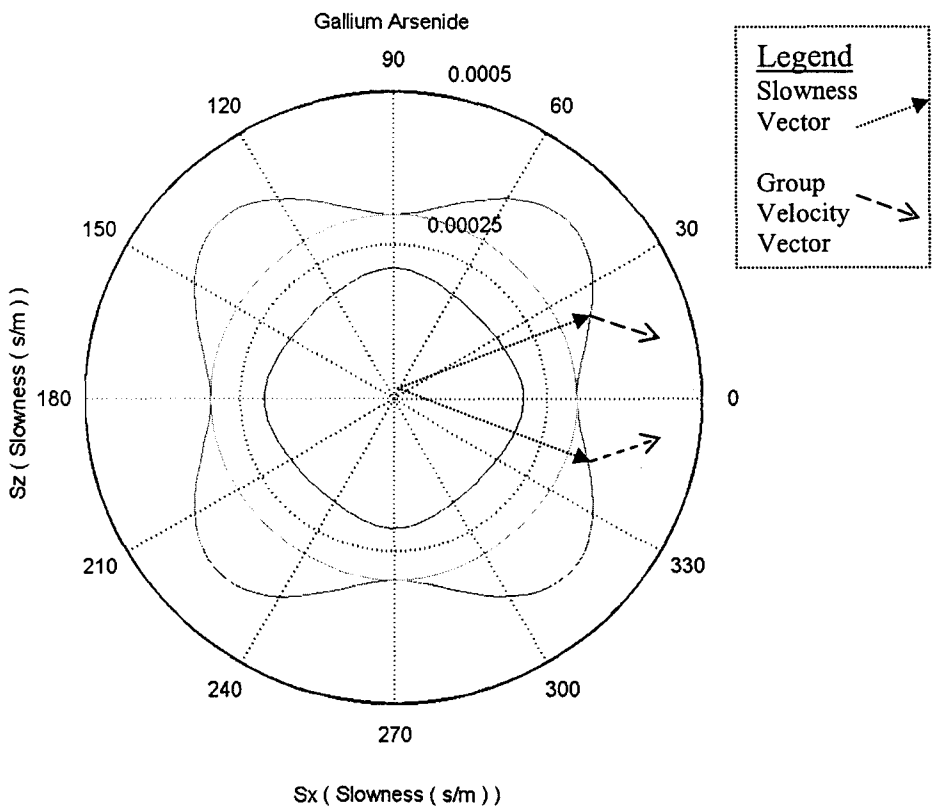

Figure 30: Group velocity vector on Slowness Curve of Gallium arsenide.

The experiments conducted and the analysis performed confirm that a stability criterion of the PML is to ensure that the slowness and group velocity vectors must not have any components that are anti-parallel. This criterion is essential to prevent the PML from exploding and thus making the FDTD simulation unstable. Also, when there is a concave section in the slowness curve, the backward energy phenomenon does not necessarily occur; however, it is a possibility.

In summary, this chapter presented a major limitation that prevents PML from becoming a global solution to the open boundary problem for acoustic waves. Nevertheless, many piezoelectric materials do not have the backward energy mode in them and therefore can be effectively simulated using the PML.

Chapter 7

7. Conclusion

This thesis presents a thorough discussion of the wave propagation and its numerical solutions in piezoelectric, elastic, and electromagnetic media. Research on this topic indicates that piezoelectric devices were in dire need of an open boundary condition. At that moment, the most efficient absorbing boundary condition (ABC) developed was the perfectly matched layer (PML). Through much research, an efficient PML was developed for piezoelectric media, and its successful demonstration is presented in this thesis.

Berenger initially developed the innovative PML in electromagnetics in 1994, intelligently using the impedance matching technique of microwave theory to generate a reflectionless layer that effectively absorbed the incoming wave. This technique was then extended to the world of acoustic wave propagation in isotropic media--a challenging task because elastic media has more than one impedance to match. However, plane wave analysis determined that as long as normal field components are attenuated, the result would be matched layer that would absorb efficiently any oblique waves in the simulation domain [4].

The PML in elastic media has been reported to give maximum relative error of below 0.1%. The PML developed in piezoelectric media gave the maximum relative

error to be less than 0.5%. This is highly acceptable because the errors are the result of numerical discretization, not a consequence of PML theory. Because of its high efficiency, the PML has now become the new standard technique for simulating any unbounded media.

While testing the PML for various piezoelectric materials, an additional stability criterion was discovered. Some materials lead to instability within the PML, producing corrupted results. It was then noticed that these anisotropic materials supported backward an energy propagation mode that carried energy opposite to propagation direction. Therefore, instead of decreasing energy in the PML region, the propagating wave actually increased energy resulting in instabilities. These materials could be known in advance by closely examining the slowness and energy velocity vectors on a slowness curve. When the slowness velocity vector had its corresponding energy velocity vector anti-parallel in any of the propagation direction, backward energy immediately resulted, leading to the possibility of an unstable PML.

This thesis presents the implementation of the PML, enabling numerical analysis of devices that use piezoelectric media. This advancement reduces time and cost for the simulation of devices that employ piezoelectric media. The efficiency of the development can be enhanced as well as the quality of the final product itself. Also, in some cases an experiment cannot be performed in which case numerical simulation provides a solution to this problem with a click of a button.

Although adequately efficient, the PML developed in this thesis still has some room for future development. Further research is needed to optimize the current PML to give minimal relative error.

Appendix

1. classes of anisotropic crystal systems

Triclinic System:

21 constants

$$\begin{bmatrix} c_{11} & c_{12} & c_{13} & c_{14} & c_{15} & c_{16} \\ c_{12} & c_{22} & c_{23} & c_{24} & c_{25} & c_{26} \\ c_{13} & c_{23} & c_{33} & c_{34} & c_{35} & c_{36} \\ c_{14} & c_{24} & c_{34} & c_{44} & c_{45} & c_{46} \\ c_{15} & c_{25} & c_{35} & c_{45} & c_{55} & c_{56} \\ c_{16} & c_{26} & c_{36} & c_{46} & c_{56} & c_{66} \end{bmatrix}$$

Monoclinic System:

13 constants

$$\begin{bmatrix} c_{11} & c_{12} & c_{13} & 0 & c_{15} & 0 \\ c_{12} & c_{22} & c_{23} & 0 & c_{25} & 0 \\ c_{13} & c_{23} & c_{33} & 0 & c_{35} & 0 \\ 0 & 0 & 0 & c_{44} & 0 & c_{46} \\ c_{15} & c_{25} & c_{35} & 0 & c_{55} & 0 \\ 0 & 0 & 0 & c_{46} & 0 & c_{66} \end{bmatrix}$$

Orthorhombic System:

9 constants

$$\begin{bmatrix} c_{11} & c_{12} & c_{13} & 0 & 0 & 0 \\ c_{12} & c_{22} & c_{23} & 0 & 0 & 0 \\ c_{13} & c_{23} & c_{33} & 0 & 0 & 0 \\ 0 & 0 & 0 & c_{44} & 0 & 0 \\ 0 & 0 & 0 & 0 & c_{55} & 0 \\ 0 & 0 & 0 & 0 & 0 & c_{66} \end{bmatrix}$$

Tetragonal System:

7 constants

$$\begin{bmatrix} c_{11} & c_{12} & c_{13} & 0 & 0 & c_{16} \\ c_{12} & c_{11} & c_{13} & 0 & 0 & -c_{16} \\ c_{13} & c_{13} & c_{33} & 0 & 0 & 0 \\ 0 & 0 & 0 & c_{44} & 0 & 0 \\ 0 & 0 & 0 & 0 & c_{44} & 0 \\ c_{16} & -c_{16} & 0 & 0 & 0 & c_{66} \end{bmatrix}$$

Tetragonal System:

6 constants

$$\begin{bmatrix} c_{11} & c_{12} & c_{13} & 0 & 0 & 0 \\ c_{12} & c_{11} & c_{13} & 0 & 0 & 0 \\ c_{13} & c_{13} & c_{33} & 0 & 0 & 0 \\ 0 & 0 & 0 & c_{44} & 0 & 0 \\ 0 & 0 & 0 & 0 & c_{44} & 0 \\ 0 & 0 & 0 & 0 & 0 & c_{66} \end{bmatrix}$$

Trigonal System:

7 constants

$$\begin{bmatrix} c_{11} & c_{12} & c_{13} & c_{14} & -c_{25} & 0 \\ c_{12} & c_{11} & c_{13} & -c_{14} & c_{25} & 0 \\ c_{13} & c_{13} & c_{33} & 0 & 0 & 0 \\ c_{14} & -c_{14} & 0 & c_{44} & 0 & c_{25} \\ -c_{25} & c_{25} & 0 & 0 & c_{44} & c_{14} \\ 0 & 0 & 0 & c_{25} & c_{14} & \frac{1}{2}(c_{11}-c_{12}) \end{bmatrix}$$

Trigonal System:

6 constants

$$\begin{bmatrix} c_{11} & c_{12} & c_{13} & c_{14} & 0 & 0 \\ c_{12} & c_{11} & c_{13} & -c_{14} & 0 & 0 \\ c_{13} & c_{13} & c_{33} & 0 & 0 & 0 \\ c_{14} & -c_{14} & 0 & c_{44} & 0 & 0 \\ 0 & 0 & 0 & 0 & c_{44} & c_{14} \\ 0 & 0 & 0 & 0 & c_{14} & \frac{1}{2}(c_{11}-c_{12}) \end{bmatrix}$$

Hexagonal System:

5 constants

$$\begin{bmatrix} c_{11} & c_{12} & c_{13} & 0 & 0 & 0 \\ c_{12} & c_{11} & c_{13} & 0 & 0 & 0 \\ c_{13} & c_{13} & c_{33} & 0 & 0 & 0 \\ 0 & 0 & 0 & c_{44} & 0 & 0 \\ 0 & 0 & 0 & 0 & c_{44} & 0 \\ 0 & 0 & 0 & 0 & 0 & \frac{1}{2}(c_{11}-c_{12}) \end{bmatrix}$$

Cubic System:

3 constants

$$\begin{bmatrix} c_{11} & c_{12} & c_{12} & 0 & 0 & 0 \\ c_{12} & c_{11} & c_{12} & 0 & 0 & 0 \\ c_{12} & c_{12} & c_{11} & 0 & 0 & 0 \\ 0 & 0 & 0 & c_{44} & 0 & 0 \\ 0 & 0 & 0 & 0 & c_{44} & 0 \\ 0 & 0 & 0 & 0 & 0 & c_{44} \end{bmatrix}$$

Isotropic System (non-anisotropic):

2 constants

$$\begin{bmatrix} c_{11} & c_{12} & c_{12} & 0 & 0 & 0 \\ c_{12} & c_{11} & c_{12} & 0 & 0 & 0 \\ c_{12} & c_{12} & c_{11} & 0 & 0 & 0 \\ 0 & 0 & 0 & c_{44} & 0 & 0 \\ 0 & 0 & 0 & 0 & c_{44} & 0 \\ 0 & 0 & 0 & 0 & 0 & c_{44} \end{bmatrix} \qquad c_{12} = c_{11} - 2c_{44}$$

References:

1. F. Chagla, C. Cabani and P. M. Smith, "Perfectly matched layer for FDTD computations in piezoelectric crystals," 2004 IEEE Ultrasonics Symposium Proceedings, Montreal, QC, pp. 517-520, 23-27 August 2004.

2. P. M. Smith and W. Ren, "Finite-difference time-domain techniques for SAW device analysis," 2002 IEEE Ultrasonics Symposium Proceedings, Munich, Germany, pp. 313-316, 8-11 October 2002.

3. A. Taflove and S. C. Hagness, Computational Electrodynamics: The Finite-Difference Time-Domain Method, 2nd Ed., Artech House, 2000.

4. F. Collino and C. Tsogka, "Applications of the PML absorbing layer model to the linear elastodynamic problem in anisotropic heterogeneous media," Geophysics, vol. 66, pp. 294-305, Jan-Feb. 2001.

5. K. S. Yee, "Numerical solution of initial boundary value problems involving Maxwell's equations in isotropic media," IEEE Trans.Antennas and Propagation, vol. 14, pp. 302-307, 1966.

6. B. A. Auld, Acoustic Fields and Waves in Solids (2nd Ed.), Kruger, 1990.

7. J. P. Berenger, "A perfectly matched layer for the absorption of electromagnetic waves," Journal of Computational Physics, vol. 114, pp. 185-200, 1994.

8. E. Becache, S. Fauqueux, P. Joly, "Stability of perfectly matched layers, group velocities and anisotropic waves," Journal of Computational Physics, vol 188, pp. 399-433, 2003.

9. W. R. Scott, C. T. Schroder, "Model for the Interaction of elastic waves with buried land mines," MURI Review, Aug. 2000.

10. Institute of Mechanical Systems, http://www.zfm.ethz.ch/alumni/leutenegger/Numerical.htm

11. "Wave Fundamentals," class notes for 12 156, Department of Physics, University of Strathclyde, Fall 2002.

12. R. A. Serway, Physics for Scientists and Engineers (4^{th} Ed.), Harcourt College Publishers, 1995.

13. Yen Liu, "Fourier analysis of numerical algorithms for the Maxwell equations," Journal of Computational Physics, Vol. 124, pp. 396-416, 1996.

14. R.M. White, D.S. Ballantine, et al., Acoustic Wave Sensors, Academic Press, 1997.